

## Special Issue Invited Review

# Photosensitizer-Mesoporous Silica Nanoparticles Combination for Enhanced Photodynamic Therapy<sup>†</sup>

Ruth Prieto-Montero , Teresa Arbeloa  and Virginia Martínez-Martínez\* 

Departamento de Química Física, Universidad del País Vasco/Euskal Herriko Unibertsitatea (UPV/EHU), Bilbao, Spain

Received 29 July 2022, accepted 9 March 2023, DOI: 10.1111/php.13802

## ABSTRACT

Mesoporous silica nanoparticles (MSNs) are widely known for their versatile applications. One of the most extended is as drug delivery systems for the treatment of cancer and other diseases. This review compiles the most representative examples in the last years of functionalized MSNs as photosensitizer carriers for photodynamic therapy (PDT) against cancer. Several commercially available photosensitizers (PSs) demonstrated poor solubility in an aqueous medium and insufficient selectivity for cancer tissues. The tumor specificity of PSs is a key factor for enhancing the PDT effect and at the same time reducing side effects. The use of nanoparticles and particularly MSNs, in which PS is covalently anchored or physically embedded, can overcome these limitations. For that, PS-MSNs can be externally decorated with compounds of interest in order to act as an active target for certain cancer cells, demonstrating enhanced phototoxicity *in vitro* and *in vivo*. The objective of this review is to collect and compare different nanosystems based on PS-MSNs pointing out their advantages in PDT against diverse types of cancers.

## INTRODUCTION

Besides surgery, chemo- or radiotherapy are conventional treatments applied against cancer. However, depending on the type of cancer an effective cure has not been found yet (1–3). Moreover, these treatments usually cause important side effects owing to their lack of selectivity for cancer cells inducing high toxicity to normal cells (4–7).

In this context, *photodynamic therapy* (PDT) is considered a complementary and minimally invasive procedure able to kill cancer cells by the cytotoxic effect emerge from the production of *reactive oxygen species* (ROS), mainly *singlet oxygen* ( $^1\text{O}_2$ ) after the photosensitizer activation by suitable light irradiation (7–12). Preclinical and clinical trials have proven PDT to be effective in early-stage tumors or the palliation of advanced

cancers, such as skin, head, neck, esophageal, or lung cancer, improving patient survival (7,8,10,13–16).

At present, although there are a wide variety of families of PSs with high singlet oxygen production (Fig. 1; [17]), few of them have been approved for PDT clinical use by the FDA.

Advanced conditions are required for PDT-PS: nontoxic in dark conditions, selectively accumulated in cancer tissues, suitable pharmacokinetics *in vivo* (related to biodistribution, stability and excretion time), intense absorption bands coefficients in the phototherapeutic window (630–850 nm) to maximize the light penetration and amphiphilic nature to ensure solubility in aqueous media and cross cell membrane ability (3,17–20). Most of the PDT-PSs belong to the porphyrin-like family. For instance, Photofrin® belongs to the first generation of PSs and although it is efficient in destroying cancer cells, its demonstrated poor selectivity to malignant tissues and long term-accumulation into the tissue (3). The second generation of PSs, *that is* Visudyne® or porphyrin-based macrocyclic structures like chlorins, bacteriochlorins or phthalocyanines, presents better antitumor effects ascribed to higher absorption coefficients and singlet oxygen quantum yield, better tumor-to-normal selectivity and shorter tissue accumulation time. Nonetheless, in some cases, the hydrophobic nature and solubility problems in aqueous media lead to molecular aggregation decreasing the potential effectiveness. Nowadays, a huge effort is devoted in the development of the third generation of PSs to enhance PDT efficiency. One strategy is based on the design of new operative PSs by rationalized chemical modification, that is by attachment (bio)targeting moieties to their molecular structure to increase water solubility and tumor selectivity (3,21). A second strategy is based on the use of *nanoparticles* (NPs) as carriers for PS (3,22–28), which serve as delivery systems able to enhance the selectivity, protect them from degradation by plasma components and increase their solubility in physiological media, lowering the required doses, increasing the therapeutic efficacy and minimizing the side effects. Besides, NPs can provide combined treatments (photodynamic-, chemo- or immuno-therapies) or imaging and diagnostic capabilities in the same nanoplatform.

There are many types of nanoparticles with potential use in biomedicine, based on different materials: metallic (gold, iron or quantum dots) and nonmetallic (micelles, liposomes, polymeric nanoparticles, carbon nanotubes or silica-based nanosystems; [3,5,29–44]). In this context, one of the most interesting nanoplatforms for transporting photosensitizers is mesoporous silica

\*Corresponding author email: virginia.martinez@ehu.eus (Virginia Martínez-Martínez)

<sup>†</sup>This article is part of a Special Issue celebrating the 50<sup>th</sup> Anniversary of the American Society for Photobiology.

© 2023 The Authors. *Photochemistry and Photobiology* published by Wiley Periodicals LLC on behalf of American Society for Photobiology.

This is an open access article under the terms of the [Creative Commons Attribution License](https://creativecommons.org/licenses/by/4.0/), which permits use, distribution and reproduction in any medium, provided the original work is properly cited.

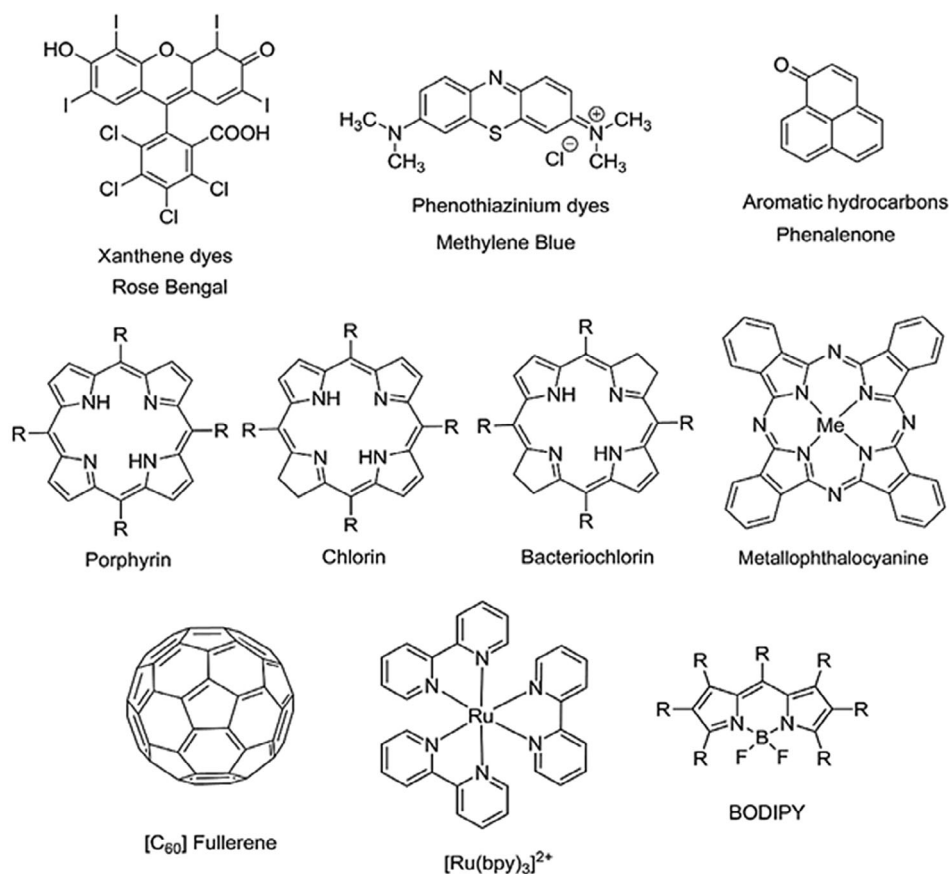


Figure 1. Molecular structure of known photosensitizers (12).

nanoparticles due to their high surface area, easy functionalization, biocompatibility, and their optical transparency, essential for PDT (22,24,38,41,45–48). In this review, we mainly focused on the use of silica mesoporous nanoparticles (MSNs) in PDT to enhance the properties of photosensitizers to destroy efficiently nearby cancer cells.

## NANOPARTICLES IN PHOTODYNAMIC THERAPY

The use of nanoparticles as carriers, which is commonly known as nanomedicine, offers many advantages: (1) their large surface to volume ratios allow the administration of a high amount of drug, (2) prevention from enzymatic degradation or inactivation of the drug by plasma components, (3) stabilization of hydrophobic drugs in the aqueous medium, and (4) enhancement the selective accumulation inside the tumor cells and their retention by enhanced permeability and retention (EPR) effect or so-called passive targeting (6,23). That is because tumor cells usually growing very fast in a more disorganized distribution and presenting large gap junctions (between 100–600 nm), allowing a greater entry of nanoparticles with respect to healthy ones. Thus, nanoparticles of a diameter size between 30–200 nm, are preferentially accumulated in the tumor cells, whereas they are unable to penetrate through tight endothelial junctions of normal blood vessels (2–20 nm). Moreover, tumors show poor lymphatic drainage, aiding longer time retention. Besides, the specificity to tumor tissues can be increased by using a particular (bio)target,

known as active targeting. By external surface functionalization with certain ligands, such as proteins, polysaccharides, nucleic acids, peptides, and small molecules, which specifically bind to receptors overexpressed in malignant cells but not in healthy cells (36,47).

Currently, there are several nanosystems approved by the (FDA), and an average of 2–3 new ones per year is being approved for specific clinical uses since 1990. Systems based on liposomes and polymeric nanoparticles were initially leading but nowadays the use of micellar, metallic or protein based nanoparticles is more extended (Fig. 2; [5,38,40]).

In the particular case of PDT, several have been used as PS transports. For instance, polymeric NPs from natural or synthetic biocompatible polymers, particularly poly(D,L-lactic-co-glycolic acid; PLGA), which degrades to biocompatible and nontoxic products and are physiologically removed from the body, have been approved by FDA to be used in humans (3,27,50,51). Other typical NPs for PS transport are liposome-based nanosystems (3,50). These nanocarriers were one of the first used in medicine and nowadays there are over 11 formulations approved for clinical use. However, they show short plasma half-time and they required extra modifications of their external surface to enhance the fast degradation before reaching the target area (3).

Apart from organic NP, metallic carriers have been also studied for PDT (50). Gold NPs have great interest due to the possibility to combine surface plasmon resonance (SPR) and the conversion of light energy to heat, what is known as Photothermal Therapy applications (PTT), with PDT. Regarding magnetic

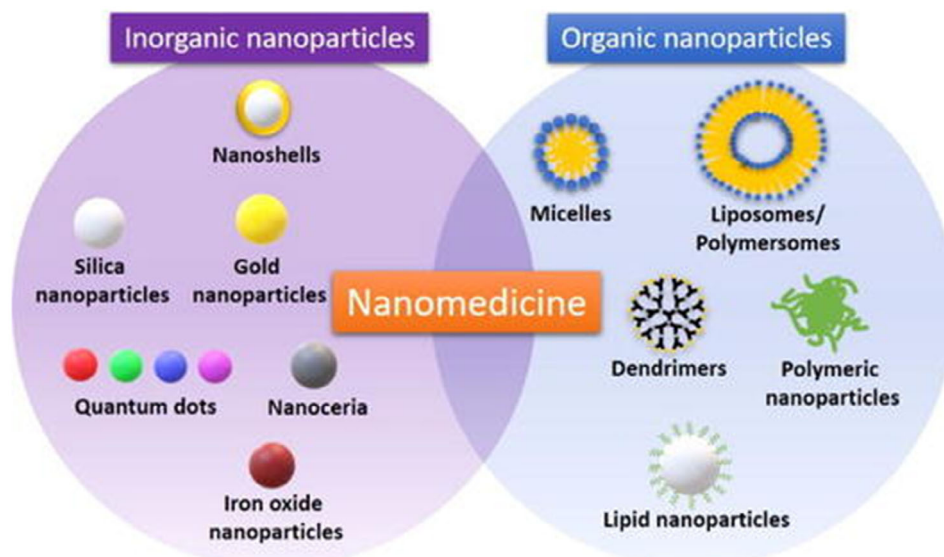


**Figure 2.** Examples of different types of nanoparticles used in biomedicine for drug transports. Source: Image taken with permission from (49).

NPs, the most common in PDT is iron oxide. In this case, these nanosystems can also provide tracking and diagnosis by magnetic resonance imaging (MRI; [3,27]).

Another type of nanoplatforms are fullerenes, a carbon allotrope with a spherical shape composed usually of 60 (C60) or 70 (C70) carbon atoms, which are sometimes considered a carrier despite their small size (approximately 0.7–1 nm). It generates high ROS species, particularly singlet oxygen (quantum yield near unity) under UV light. Unfortunately, UV light is not suitable irradiation for human tissues, being responsible for DNA damage and genetic defects or mutations (3,27,52–54).

Finally, silica NPs, mainly with mesoporous structure (MSNs), are also widely used, and could be considered one of the most interesting nanocarriers for PSs due to its optical transparency to light absorption and biocompatibility (3,32,50,55).

### MESOPOROUS SILICA NANOPARTICLES: TYPES, SYNTHESIS AND FUNCTIONALIZATION

The silica nanoparticles can be classified into three different types: (1) Stöber silica nanoparticles (56), (2) organically modified silica (ORMOSIL) and (3) mesoporous silica nanoparticles (MSN). These different types are differentiated based on their structure or nature of core; without porous structure (nonporous), with porous of few nanometers (mesoporous) or a more organophilic core by the combination of different silica sources (ormosil). Note here, any of the three types of silica nanoparticles can enclose functionalized shells (Fig. 3).

Among these three types, nonporous silica nanoparticles were the first one on which the method was developed to control nanoparticle growth, shape, and distribution in 1986 by Stöber and Fink, currently known as the Stöber method (56). This is based on the sol-gel process, starting from an alkoxide (tetraethoxysilane, tetramethoxysilicate or others) in a water/ethanol mixture and using ammonium hydroxide as a catalyst. As a result, monodisperse, spherical and electronically stabilized silica nanoparticles are obtained by hydrolysis and condensation reactions (Fig. 4).

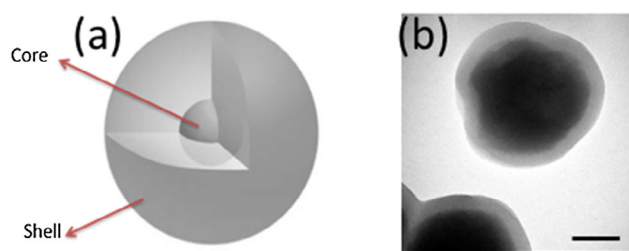


**Figure 3.** (a) Schematic representation of core-shell structure sphere nanoparticles; (b) TEM image of a mesoporous silica nanoparticle with core-shell structure, scale bar = 50  $\mu\text{m}$ .

In the other two types: ormosil and mesoporous, modifications in the Stöber method are required. For ormosil nanoparticles, a second silica source with a more organophilic character is used (36,57). Regarding MSN, the addition of a cationic surfactant into the synthesis gel is required to act as a template and through micelle formation, pores are generated with a size range from 2 to 50 nm, after removing the surfactant (58,59). As a result, the MSNs present two areas of work, the mesoporous structured core and their external surface, in which different drugs and targeting moieties would be accommodated (Fig. 3). For that reason, MSNs are considered more versatile than nonporous silica NPs. Besides, MSNs could be synthesized with different shapes: sphere-like, yolk-shell, hollow and peanut-like structures, being sphere nanostructures preferred for their use as carriers (60–63). Their potential use as a drug delivery system was firstly proposed by Vallet-Regí in 2001 (64). So far, the great increase in the number of publications about these nanosystems, demonstrates they fulfill the crucial requirements for their use in nanomedicine.

Regarding their synthesis, nowadays, many different works described the effect of reaction conditions on the size, morphology, and distribution of mesoporous silica nanoparticles. In general, five parameters are mainly considered; (1) temperature, (2) pH value, (3) silica source concentration and nature (4) type of

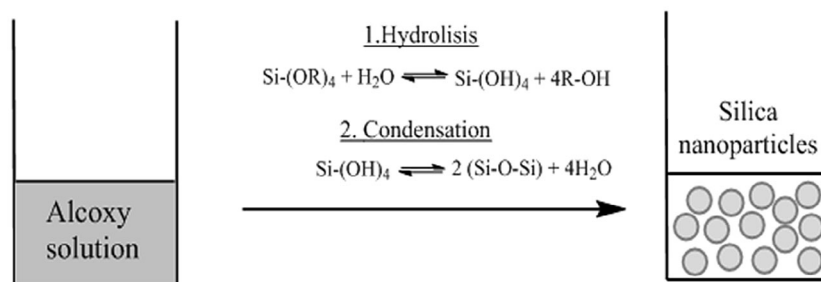


**Figure 4.** Scheme of Stober method; hydrolysis and condensation reactions.

alcoholic solvent used and (5) surfactant type and concentration (46). The variations of these conditions induce a modification of the NP size ranging from 25 nm to 2  $\mu\text{m}$  (Fig. 5). Thus, all these factors have to be taken into account in the synthesis of mesoporous silica nanoparticles:

- 1 Temperature. In general terms, MSNs size tends to decrease when the reaction temperature increases. For example, Lin *et al.* (59) obtained MSN with 260 nm at 30°C, while the diameter size of 24 nm reached at 60°C was drastically reduced.
- 2 pH. This parameter has a great impact on the hydrolysis of the silica source, being faster as pH increases. Conversely, the condensation is not directly related to pH and is favored at pH values between 7.5–8.4. For that reason, at a low pH, the reaction time becomes very slow modifying the NP morphology and size. In this regard, different bases could be used, being the most common ammonium hydroxide ( $\text{NH}_4\text{OH}$ ) or sodium hydroxide ( $\text{NaOH}$ ; [46,59,60]).
- 3 Alkoxide concentration. It is proportional to the size of nanoparticles, meaning that if the concentration raises, the size of the nanoparticles does too (59). In the case of the silica source

type, the shorter the carbon chain the smaller the size of the nanoparticles, attributed to a less steric effect during the nucleophilic attack by water (46).

- 4 Alcohols as a cosolvent. It facilitates the alkoxy solution. Note that long-chain alcohols lead to high nanoparticles size and wider size distribution. For this reason, obtaining smaller and more homogeneous nanoparticles, methanol or ethanol is convenient (59).
- 5 Surfactant. It is crucial to obtain the characteristic mesoporous nature inside the nanoparticles, which is the result of complex interactions between the micelles and the silica oligomers during condensation. The surfactant concentration affects the hydrolysis and its micellization. Generally, MSN presents a more homogenous and spherical distribution at lower concentrations of surfactant. The most typically used are salts of dodecyl or cetyltrimethylammonium (CTA), such as cetyltrimethylammonium chloride (CTAC) or cetyltrimethylammonium bromide (CTAB; [60]).

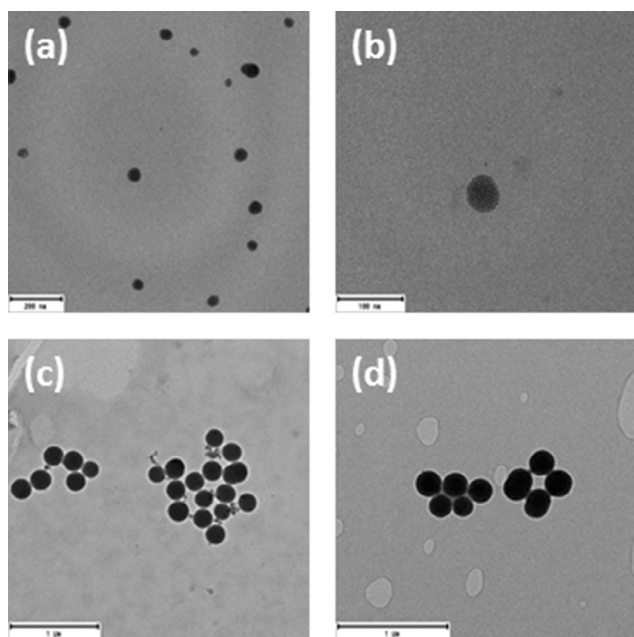
The mesoporous nature is an essential parameter in MSN and implies a new area of functionalization. To exploit this inner mesoporous structure, surfactant has to be previously removed, commonly by (1) calcination (46,65,66) or (2) acid treatment (67–69).

Interestingly, both areas (external and internal surfaces) of mesoporous silica nanoparticles can be easily functionalized (38,70,71). In this context, depending on the functional groups required, different silica sources are available (Table 1).

The presence of different organic groups opens the opportunity to chemically tether a great number of compounds of interest (drugs, biomolecules, biopolymers) in the shell or/and in the core of the nanoparticles (68,72–74). In many cases, only one of the two areas is selectively functionalized. MSN allows multiple combinations to carry the different molecules of interest. For example, some components could be physically embedded in the pores without any covalent union (36), whereas others could be covalently anchored at the external functionalized shell (66,69,75–80).

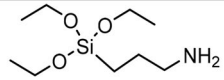
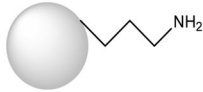
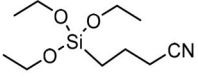
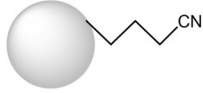
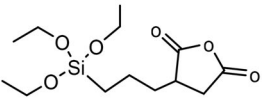
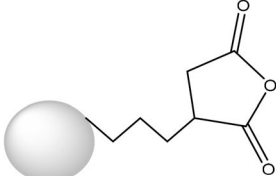
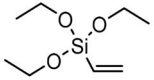
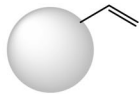
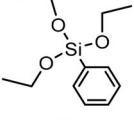
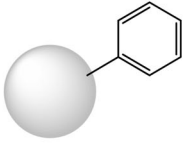
## BIOCOMPATIBILITY AND BIODISTRIBUTION STUDIES OF MESOPOROUS SILICA NANOPARTICLES

*In vivo* studies carried out in mice related to pharmacokinetics of MSN have revealed very promising results for their implementation into clinical trials. In this section general trends are detailed since the outcomes usually depend on their size and morphology and chemical composition, besides the injected dosage and



**Figure 5.** TEM images of MSN of different size for an example: 50 nm (a,b) and 250 nm (c,d).

**Table 1.** Examples of the different alkoxysilane sources available and their corresponding functional group at the nanoparticle.

Alkoxysilane source	Functionalization in nanoparticle
 <p>APTES 3-aminopropyltriethoxysilane</p>	
 <p>CTES 3-Cyanopropyltriethoxysilane</p>	
 <p>TESPSA (3-Triethoxysilyl)propylsuccinic anhydride</p>	
 <p>VTES triethoxyvinylsilane</p>	
 <p>PTES phenyltriethoxysilane</p>	

expose-routes (oral, intravenous, subcutaneous, intraperitoneal or intramuscular administrations; [81,82]). As an example, MSNs of around 50 nm diameter and different functionalities at the external surface (OH-, COOH or PEG- groups) displayed different blood circulation times, being pegylated particles those with longer retention times, lower liver uptake and reduced toxicity, as have been generally observed for other PEG-decorated nanoparticles (82). In general terms, *in vivo* studies have demonstrated that MSNs of diameter between 50–200 nm are preferentially accumulated into tumor tissues due to EPR effect. In addition, this selectivity was further promoted by conjugation with specific small molecules, ligands or antibodies at their external surface (83,84).

According to the toxicological profile of MSNs, dosage of 50 mg kg<sup>-1</sup> is considered nontoxic and can be safely used (81,83,85). However, coating strategies are also able to reduce toxicity and higher doses might not reveal toxic effects (82). As mentioned above, the excretion process is closely related to the distribution of MSNs and the administration method. On average, *in vitro* studies indicated that MSNs are evacuated out of the body through renal and fecal routes, and a complete clearance is typically reached between 4 to 7 days after injection (81,83).

Although *in vivo* biocompatibility profile of MSNs is still very limited and further studies should be completed, these preliminary findings impart MSNs as suitable nanovehicles of PSs to

overcome some of their limitations, such as low selectivity to malignant tissues or long term-accumulation into the tissue (even for weeks). MSN has also allowed the combination of PDT with other therapies and can be provided with bioimaging capabilities. Many studies, through *in vitro* and *in vivo* experiments, have demonstrated their potential applicability in the nanomedicine field. Different examples of PS-MSN systems and their benefits in the PDT implementation are detailed below.

## PHOTOSENSITIZERS LOADED IN SILICA NANOPARTICLES

Mesoporous silica nanoparticles has been used as carrier for PS, and different types of photosensitizers have been tethered outside or encapsulated inside. Moreover, many targets are used in other to tackle different types of cancers. In this review, we have focused on recent works on the applicability of MSN as PS-vehicles for PDT. In the following sections, the most representative examples are divided by the type of PS used.

### Porphyrins

One of the most studied type of PSs is the porphyrin family. As mentioned above, the first PS applied in clinical trials was Hematoporphyrin (86–88). In fact, a great number of studies

were carried out with PSs derivative of this family. For example, Bouffard *et al.* encapsulate a neutral porphyrin (bearing a maleimide arm) inside MSN of 130 nm diameter, to use against prostate cancer in cell culture. (89) Mannose was selected as a specific target and the effect of this target on the phototoxic efficiency was analyzed by comparing three different designed nanoparticles: (1) without target (MSN), (2) with one molecule of mannose (MNS-M6C) and (3) with dimannoside derivative (MSN-M6C-Man) in Human prostate adenocarcinoma cells (LNCaP). They exposed the cells to the three nanosystems at the same concentration of  $80 \mu\text{g mL}^{-1}$  at different incubation times (Fig. 6), and cells were irradiated for 20 min under 650 nm (3 mW,  $11.25 \text{ J cm}^{-2}$ ). Their experiment showed a higher effect of dimannoside derivative at lower times, being MSN-M6C-Man able to destroy 73% of the cells while MSN-M6C and MSN only 35% and 10%, respectively, for 6 h of incubation. It was a good example of how a better affinity to the cancer cell receptors enhances the phototoxicity effect of the nanoparticles *in vitro* (89).

Bretin *et al.* in 2019 (6) also tethered a porphyrin, 5-(2-[3-carboxypropyloxy] phenyl)-10,15,20-triphenylporphyrin (TPPOH), in the surface of silica nanoparticles of 80 nm diameter to treat human colorectal cancer (CRC). They used a hemicellulose (xylan) as a bridge to control the TPPOH delivery. (90) Xylan is natural, biodegradable, and nontoxic biomaterial, which improves the biodistribution of the nanosystem. Bretin *et al.* compared the toxicity of the new hybrid nanosystem with respect to TPPOH-free in solution both under dark and irradiation conditions through *in vitro* experiments in three human CRC cell lines: (1) HT-29 (2) HCT116 and (3) SW620.

After exposing the cells to red irradiation (630–660 nm) and analyzing the phototoxicity 48 h later, similar tendencies were found in the three cell lines: both TPPOH-free and TPPOH-@NP (TPPOH-X-SNPs) were nontoxic under dark conditions but the phototoxicity showed by the nanosystem were higher than TPPOH-porphyrin in solution, Table 2. HCT116 and SW620 showed the same  $\text{IC}_{50}$  whereas HT-29 cells were relatively most resistant to the phototreatment according to their higher  $\text{IC}_{50}$  value, Table 2 (6).

The analysis of the internalization and colocalization *in vitro* of the TPPOH@nanosystem and free TPPOH inside HT-29 cells (Fig. 7), at the same concentration ( $1 \mu\text{M}$ ), determined a much

higher uptake of TPPOH-X-SNP with respect to TPPOH in solution, particularly 98.8% vs a 2.32%, after 24 h of incubation. Similar, results were obtained at 2, 6, and 12 h of postincubation and for the other two cell lines. The colocalization test indicated that nanosystems preferably colocalized with lysosomes (50.8%), although to some extent also in mitochondria (12%) for HT-29 cells, alike for HCT116 and SW620.

This group has also studied the antitumor efficacy *in vivo*, demonstrating an increased apoptosis and cell proliferation inhibition after the injection of TPPOH (@NP and free in solution). The accumulation capability of TPPOH-X-SNP and TPPOH inside the tumors was analyzed 24 h postinjection. TPPOH-free (red circles) showed a minimal accumulation at tumor sites in contrast to TPPOH-X-SNP (Fig. 8). The *ex-vivo* fluorescence imaging of tumors and major organs at 24 h postinjection indicated a higher accumulation in the liver and kidney with respect to other organs or tumors, confirmed by quantitative ROI analysis.

Li *et al.* (91) also considered the MSN, in this case of 88 nm diameter, a suitable nanotransport for porphyrin. In this case, 5,10,15,20-tetrakis (1-methyl 4-pyridinio) porphyrin tetra (p-toluenesulfonate) (TMPyP) was encapsulated inside the mesoporous of MSN, together with silicon nanoparticles (SiNPs) during the MSN synthesis to attain two-photon fluorescence for bioimaging. Moreover, they analyzed the possibility of combining PDT with chemotherapy, by coadsorbing doxorubicin (DOX), a widely known anticancer drug, inside the mesoporous core. They have targeted Human Breast Carcinoma and Human Lung Cancer by studying MCF-7 and A549 cell lines, respectively. To enhance the specific selectivity of the nanosystems, Li *et al.* tethered Folic Acid at the MSN surface. Briefly, Folic Acid (FA) is a small molecule widely used as a target for a great number of cancer cells to enhance selectivity (74,92,93).

The internalization of MSN without DOX (Fig. 9) was analyzed by recording the fluorescence of SiNPs by two-photon excitation with 800 nm laser as excitation source. The lower blue fluorescence emission for A549 cells in comparison with MCF-7 cells was attributed to a lesser number of folate receptors in this cell line (91). To evaluate the (photo)toxicity in MSNs were incubated in culture media at different concentrations ranging from 0 to  $100 \mu\text{g mL}^{-1}$  and irradiated at 655 nm with a dose light of  $27 \text{ J cm}^{-2}$  ( $300 \text{ mW cm}^{-2}$  during 90 s). The

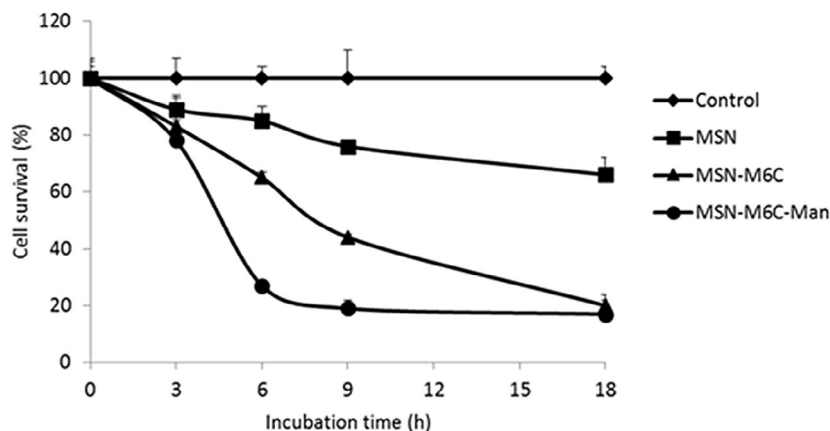


**Figure 6.** LNCaP cell survival after incubation with MSN, MSN-M6C, or MSN-M6C-Man and irradiation at 650 nm. Source: Figure taken with permission from (89).

**Table 2.** Summary table of PS-MSNs hybrid systems used *in vitro* assays.

System	Diameter (nm)	PS position	Target	Cell Line	Irradiation Light (nm)	Power (J cm <sup>-2</sup> )	IC <sub>50</sub> MSN	IC <sub>50</sub> Free	REF
TPPOH-XSNP	80	Outside	Xylan	HT-29 (CRC)	630–660	75	0.55 μM	6 μM	(7)
TPPOH-XSNP	80	Outside	Xylan	HCT116 (CRC)	630–660	75	0.073 μM	3 μM	(7)
TPPOH-XSNP	80	Outside	Xylan	SW620 (CRC)	630–660	75	0.075 μM	3 μM	(7)
MSN@SiNPs@TMPyP-FA	88	Inside	FA	MCF-7 (Breast)	655	27	80 μg mL <sup>-1</sup>	-	(92)
MSN@SiNPs@TMPyP-FA/DOX	88	Inside	FA	MCF-7 (Breast)	655	27	60 μg mL <sup>-1</sup>	-	(92)
MSN@SiNPs@TMPyP-FA/DOX	88	Inside	FA	A549 (Lung)	655	27	90 μg mL <sup>-1</sup>	-	(92)
MSN	130	Inside	-	LNCaP (prostate)	650	11.25	-	-	(90)
MSN-M6C	130	Inside	mannose	LNCaP (prostate)	650	11.25	-	-	(90)
MSN-M6C-Man	130	Inside	dimannoside derivivate	LNCaP (prostate)	650	11.25	-	-	(90)
MSNNR@MoS <sub>2</sub> -HSA/Ce6	200	Outside	Human serum album	4T1 (mammary carcinoma)	808/660	450/300	≈80 μg mL <sup>-1</sup>	200 μg mL <sup>-1</sup>	(95)
MSN-Ce6-FA	150–180	Outside	FA	MDA-MB-231 (breast)	670	60	≈2 μM	>5 μM	(40)
Ce6@MSN	50	Outside	FA	HeLa (cervical tumor)	655	15	5.3 μM 890 μg mL <sup>-1</sup>	0.7 μM	(83)
Ver-MSN	160–180	Both	-	HaCaT (normal human keratinocyte)	650	-	-	-	(96)
Ver-MSN	160–180	Both	-	A375P (a low metastatic melanoma)	650	-	-	-	(96)
Ver-MSN	160–180	Both	-	SK-MEL-28 (highly invasive melanoma)	650	-	-	-	(96)
RB@HMSNNs-N=C-HA	170	Inside	HA	4T1 (mammary carcinoma)	532	3	8.89 μg mL <sup>-1</sup>	9 μg mL <sup>-1</sup>	(108)
RB-DOX@HMSNNs-N=C-HA	170	Inside	HA	4T1 (mammary carcinoma)	532	3	0.23 μg mL <sup>-1</sup>	9 μg mL <sup>-1</sup>	(108)
RB@MSN	50	Outside	FA	HeLa (cervical tumor)	518	10	0.55 μM 27 μg mL <sup>-1</sup>	1.04 μM	(83)
MSN-I <sub>2</sub> -BDP-PEG	90	Outside	-	HeLa (cervical tumor)	500	4.8	5 μg mL <sup>-1</sup>	-	(24)
BDP1-NP	50	Outside	FA	HeLa (cervical tumor)	435	10	1.1 μM 36 μg mL <sup>-1</sup>	-	(83)
BDP3-NP	50	Outside	FA	HeLa (cervical tumor)	518	10	0.4 μM 10 μg mL <sup>-1</sup>	<0.1 μM	(83)
BDP4-NP	50	Outside	FA	HeLa (cervical tumor)	518	10	0.4 μM 88 μg mL <sup>-1</sup>	4 μM	(83)
BDP5-NP	50	Outside	FA	HeLa (cervical tumor)	518	10	0.1 μM 10 μg mL <sup>-1</sup>	4 μM	(83)
BDP6-NP	50	Outside	FA	HeLa (cervical tumor)	655	10	<0.1 μM <14 μg mL <sup>-1</sup>	<0.1 μM	(83)
ID@HMSNs-B-HA	170	Inside	HA	4T1 (mammary carcinoma)	808	600	1.35 μg mL <sup>-1</sup>	>16 μg mL <sup>-1</sup>	(46)
MSN-PEG@Cur	100	Inside	-	HeLa (cervical tumor)	430	36	5.5 μg mL <sup>-1</sup>	22.9 μg mL <sup>-1</sup>	(13)
G-Ru3	200	Inside	-	MRC-5 (Noncancerous Human Normal Lund Fibroblast)	480	8.7	66 μg mL <sup>-1</sup> 57 nM	1500 nM	(115)
G-Ru-4	200	Inside	-	MRC-5 (Noncancerous Human Normal Lund Fibroblast)	480	8.7	44 μg mL <sup>-1</sup> 48 nM	2400 nM	(115)
					540	9.5	74 μg mL <sup>-1</sup> 49 μg mL <sup>-1</sup> 54 nM	3700 nM	

(continued)

**Table 2.** (continued)

System	Diameter (nm)	PS position	Target	Cell Line	Irradiation Light (nm)	Power (J cm <sup>-2</sup> )	IC <sub>50</sub> MSN	IC <sub>50</sub> Free	REF
G-Ru3	200	Inside	-	A2780 (Cancerous Human Ovarian Carcinoma)	480	8.7	72 µg mL <sup>-1</sup>	2200 nM	(115)
					540	9.5	62 nM 83 µg mL <sup>-1</sup>	2900 nM	
G-Ru-4	200	Inside	-	A2780 (Cancerous Human Ovarian Carcinoma)	480	8.7	71 nM 51 µg mL <sup>-1</sup>	2700 nM	(115)
					540	9.5	56 nM 64 µg mL <sup>-1</sup>	3300 nM	
G-Ru1	200	Inside	FA	MRC-5 (Noncancerous Human Normal Lund Fibroblast)	480	8.7	>500 µg mL <sup>-1</sup>	1500 nM	(115)
					540	9.5	>133 nM >500 µg mL <sup>-1</sup>	3700 nM	
G-Ru-2	200	Inside	FA	MRC-5 (Noncancerous Human Normal Lund Fibroblast)	480	8.7	>133 nM >500 µg mL <sup>-1</sup>	2400 nM	(115)
					540	9.5	>360 nM >500 µg mL <sup>-1</sup>	5600 nM	
G-Ru1 /G-Ru-2	200	Inside	FA	A2780 (Cancerous Human Ovarian Carcinoma)	480	8.7	159 µg mL <sup>-1</sup>	2200 nM	(115)
					540	9.5	42 nM 187 µg mL <sup>-1</sup>	2900 nM	
G-Ru1/G-Ru-2	200	Inside	FA	A2780 (Cancerous Human Ovarian Carcinoma)	480	8.7	50 nM 43 µg mL <sup>-1</sup>	2700 nM	(115)
					540	9.5	31 nM 61 µg mL <sup>-1</sup>	3300 nM	

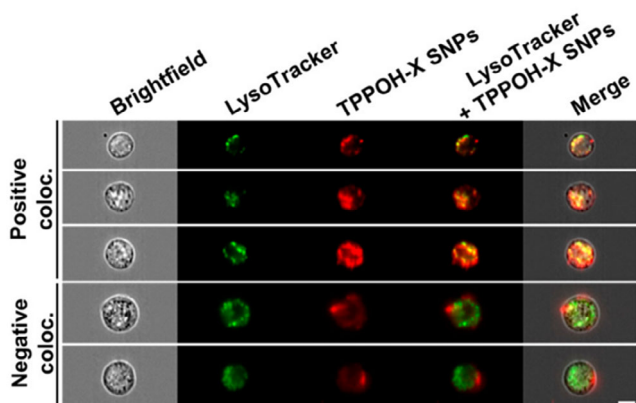


**Figure 7.** Assay carried out by Bretin *et al.* Representative images of colocalization of TPPOH-X SNPs and LysoTracker in HT-29 cells are shown. Source: Figure taken with permission from (6).

nanosystems without DOX did not present any toxicity in dark, and around 80% of the cells survived at the highest concentration (100 µg mL<sup>-1</sup>). When the nanosystems were incubated and irradiated, a concentration of 90 µg mL<sup>-1</sup> was required to obtain the 50% of the cell death in A549, whereas a lower concentration of 60 µg mL<sup>-1</sup> was needed in MCF-7. This result demonstrates the importance of an adequate target to obtain good internalization of nanosystems inside the cells. Finally, adding the combination of DOX and PS the effectivity of the NPs against cancer slightly increases, reaching 50% of cell death at 80 and 60 µg mL<sup>-1</sup>, respectively (Table 2; [91]).

Alternatively to these porphyrins, another common PS in PDT is chlorin e6 (Ce6). It has been widely used in the last years, for example by Yang *et al.* (94), Bharathiraja *et al.* (41) and our group (79). Yang *et al.* covalent anchored this PS to MSN together with Human Serum Albumin (HSA) as a target for breast cancer. Their nanoparticles of 200 nm size were also combined with molybdenum disulfide MoS<sub>2</sub> (a graphene-like 2D nanomaterial), encapsulated in the core as photothermal agent under 808 nm laser in order to combine both therapies. 4T1 breast cancer cell line was incubated with (1) free Ce6 in solution, (2) MSN with MoS<sub>2</sub> and HSA (without Ce6) and finally (3) the complete system (MSNNR@MoS<sub>2</sub>-HSA/Ce6). Under dark conditions cell viability above 80% was obtained even at the highest concentration (200 µg mL<sup>-1</sup>), demonstrating a lack of toxicity. However, under different light irradiations (660 nm at 300 J cm<sup>-2</sup>, 808 nm at 450 J cm<sup>-2</sup> and both simultaneously), demonstrated a synergetic effect between both therapies by increasing the effectivity of the complete nanosystem (MSNNR@MoS<sub>2</sub>-HSA/Ce6) with respect to separated ones (*i.e.* ≈ 60% of the cells survival at 100 µg mL<sup>-1</sup> for Free Ce6 and MSNNR@MoS<sub>2</sub>-HAS vs 40% for in the complete MSNNR@MoS<sub>2</sub>-HSA/Ce6 nanosystem; [94]). The *in vivo* assays also demonstrated the prolongation of half-life of Ce6 when linked to MSN, as well as a better specificity for the tumor by the presence of HSA on their surface (94).

Bharathiraja *et al.* (41), also covalent anchored Ce6 at the outside surface of MSN of 150–180 nm together with folic acid as a target, likewise Li *et al.* (91) Bharathiraja *et al.* also analyzed the effect of folic acid on the internalization into MDA-MB-231 breast cancer cell line with folate receptors (Fig. 10). They found that MSNs were not internalized when FA was added to the



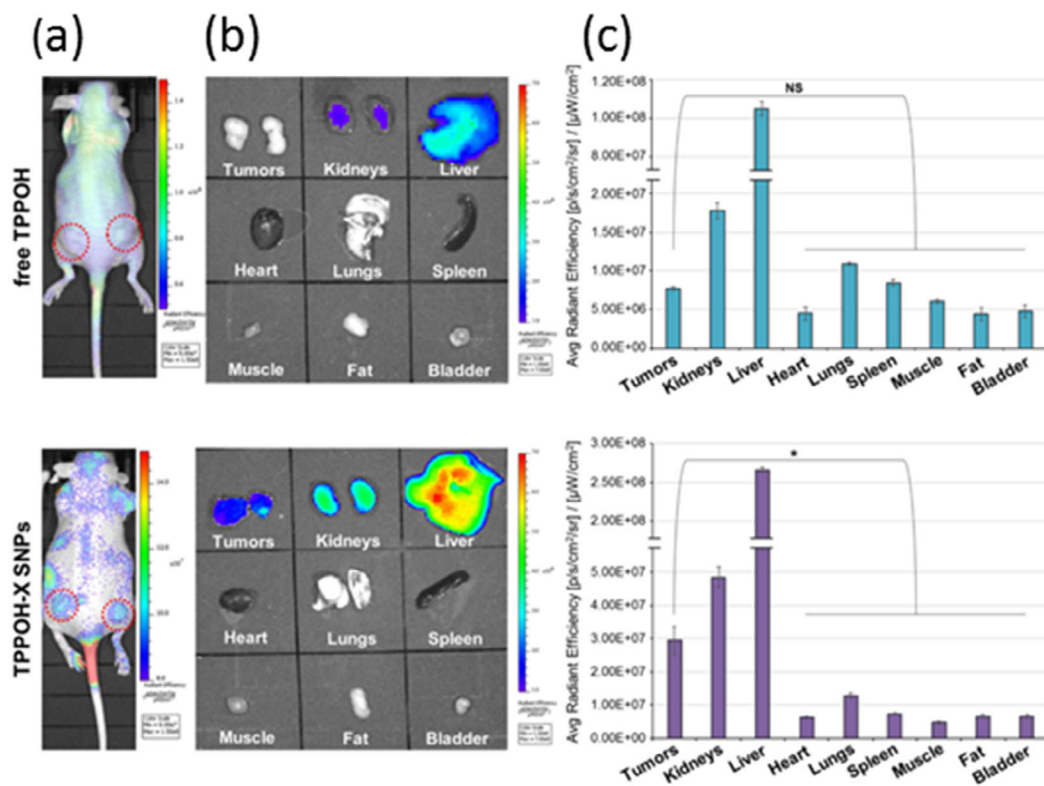


**Figure 8.** Assay carried out by Bretin *et al.* (a) *In vivo* fluorescence imaging of HT-29 tumor-bearing mice at 24 h postintravenous injection of Cy5.5-labeled free TPPOH and TPPOH-X SNPs, at 1/100 LD<sub>50</sub> for each group. The red circles indicate tumor sites. (b) *Ex-vivo* fluorescence imaging of tumors and organs at 24 h postinjection. (c) ROI analysis of fluorescence intensity of tumors and organs at 24 h postinjection. Source: Figure taken with permission from (6).

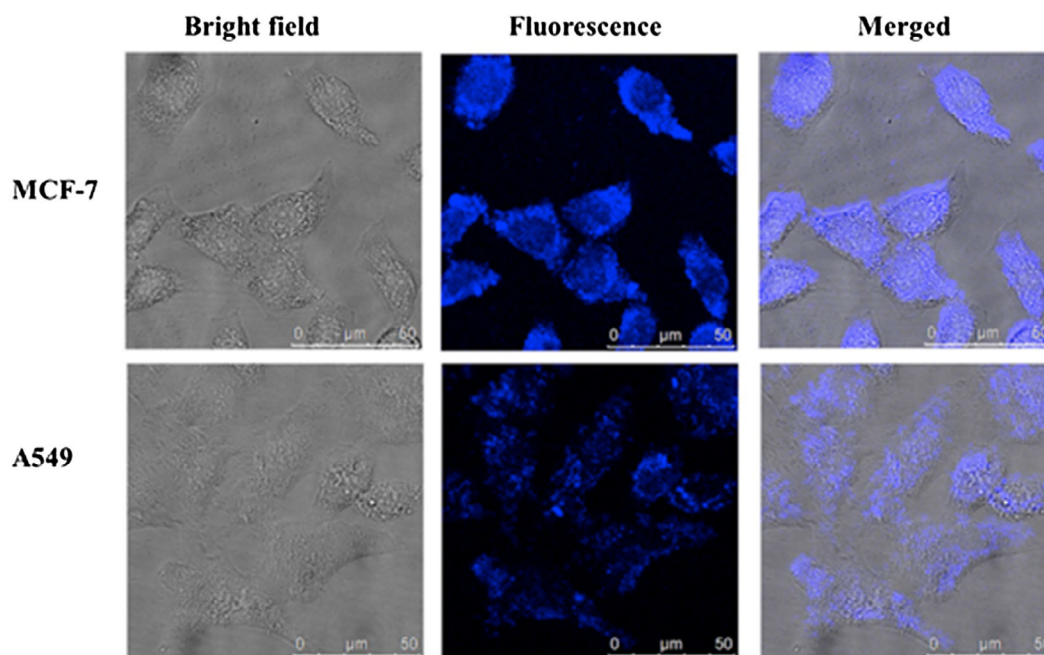


**Figure 9.** Bright field (left), two-photon fluorescence (middle) and merge (right) images of MCF-7 cells and A549 cells incubated with 80 μg mL<sup>-1</sup> of MSN@SiNPs@TMPyP-FA for 6 h excited by the 800 nm laser. The bar size is 50 μm. Source: Figure taken with permission from (91).

culture media, as a consequence of the folate receptors were already linked to that free-FA (41). Regarding HepG2 (Fig. 10), a cell line from the liver without folate receptors, the MSNs were

either internalized, demonstrating the importance of the specific target for every type of cancer. These MSNs did not show any toxic effect in dark conditions even at a relatively high

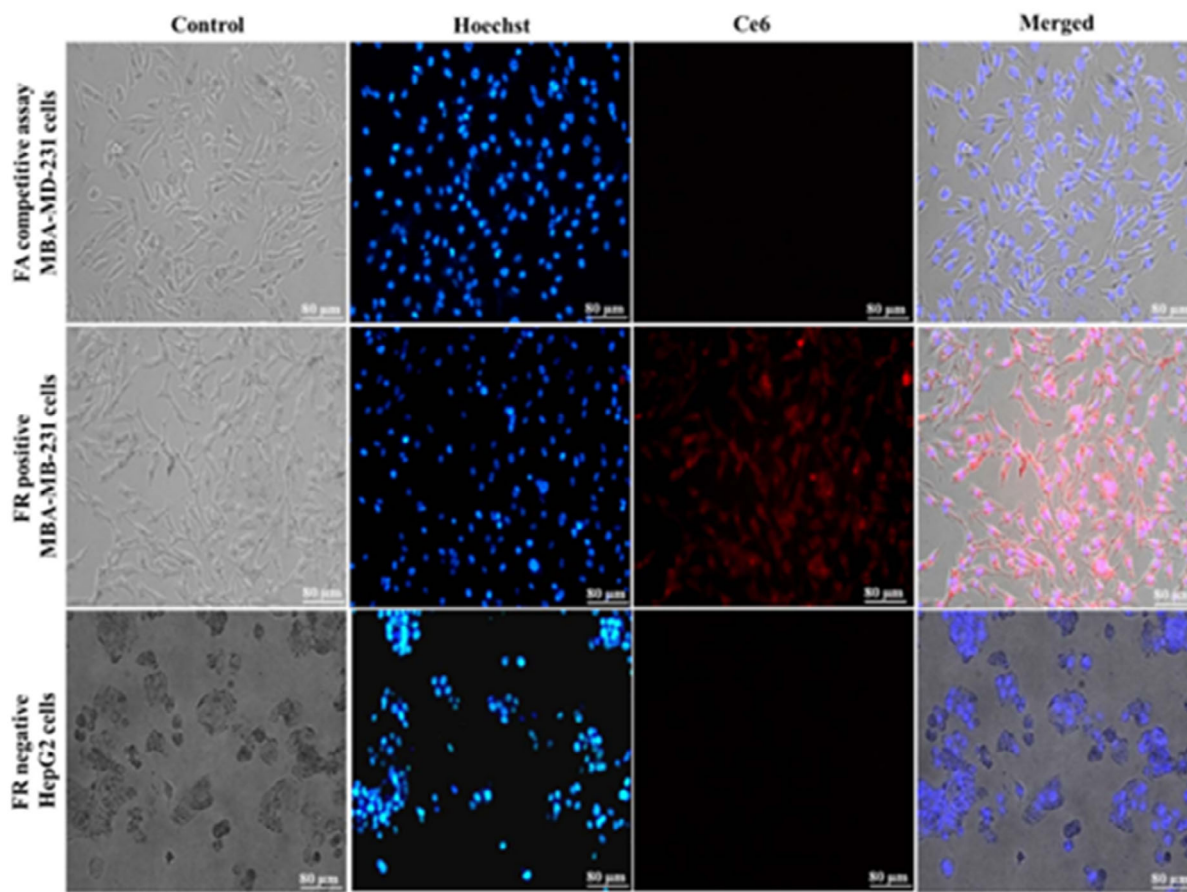


**Figure 10.** Cellular uptake of silica-Ce6-FA ( $50 \mu\text{g mL}^{-1}$ ) by MDA-MB-231 cells in the presence and absence of 1 mM free folic acid and uptake activity by HepG2 cells. Source: Figure taken with permission from (41).

concentration ( $100 \mu\text{g mL}^{-1}$ ) in MDA-MB-231 cells whereas under light illumination evidenced a clear difference between the free-Ce6 and anchorage to MSN, being Ce6@MSN considerably more phototoxic in cell culture ( $\text{IC}_{50} \approx 2 \mu\text{M}$  in MSN vs  $\text{IC}_{50} > 5 \mu\text{M}$  in solution), Table 2 (41).

Our group has also worked with the Ce6 tethered to the external surface of MSN of 50 nm diameter, together with PEG (of 2000 Da) to ensure a homogeneous dispersity of MSNs in water, and Folic Acid as biotarget for HeLa cancer cells (79). A previous study carried out in our group, demonstrated how the presence of FA increased the internalization of these pegylated MSNs inside HeLa cells up to 20% at  $1 \mu\text{g mL}^{-1}$  (36). In this case, the singlet oxygen quantum yield of Ce6 was unaffected when it was linked to the external shell of MSNs indicative of no molecular aggregation at the nanoparticle surface. *In vitro* studies in HeLa cells were performed for Ce6@MSN and Ce6-free in solution at normalized concentrations from 0 to  $10 \mu\text{M}$ . The dark toxicity found for Ce6-free in solution ( $\text{IC}_{50} = 81 \mu\text{M}$ ) was removed when it was at the MSN external surface. Besides Ce6@MSN demonstrated a better phototoxicity efficiency than Ce6-free after the irradiation at  $655 \text{ nm}$  ( $15 \text{ J cm}^{-2}$ ; Table 2).

Another common porphyrin-like PS used in PDT is Verteporfin (Ver). Rizzi *et al.* published a work that analyzed the phototoxicity of this PS covalently linked to MSN in three different cell lines: (1) a normal human keratinocyte (HaCaT), (2) a low metastatic melanoma (A375P) and (3) a highly invasive

melanoma (SK-MEL-28). The phototoxic effect under red irradiation at different light exposure times was compared in culture media (95).

They demonstrated that Ver-MSN reduced the proliferation of SK-MEL-28 to 40% under 180 s of irradiation with a standard tungsten-halogen lamp (75 W) and a 650/8 filter. In the contrast, negligible effects were detected under irradiation in the proliferation of the other two cell lines. In line with this, SK-MEL-28 cells underwent a clear change in morphology when they were exposed to Ver-MSN, but this phenomenon was not appreciated in the other two cell lines (HaCaT and A375P; Fig. 11). The authors attribute the different behavior to a greater Enhanced Permeability and Retention (EPR) effect in highly invasive melanoma cell lines, which according to Joffre *et al.*, the endocytic ability is directly correlated to tumor invasiveness (95,96).

### Xanthenes

Another family of PS widely known is the xanthene-type dyes. Particularly, Rose Bengal (RB) (Fig. 1), is extensively used as a singlet oxygen reference (79,97–104). According to its absorption range (no absorbance above 600 nm), RB is not considered a suitable PS for PDT. However, it has been demonstrated that its PDT efficiency can be enriched by formulation, that is occluded in lipid nanovesicles or chemically modified by covalently attaching an amphipathic peptide, showing a potential use

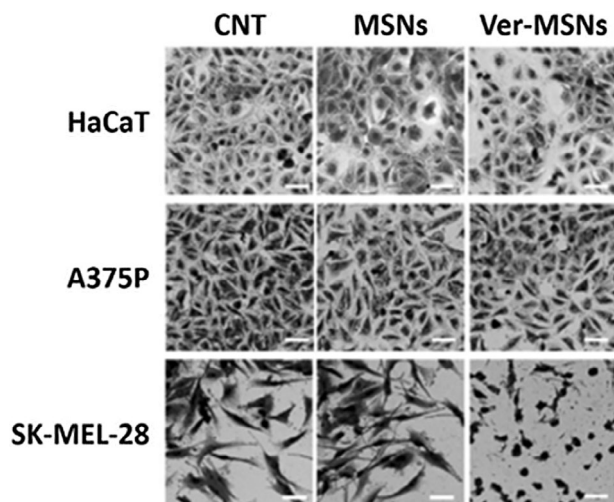


**Figure 11.** PDT effects on cell proliferation. Optical microscopy images magnification =  $10\times$ . CNT, control; MSNs, plain mesoporous silica nanoparticles ( $10\ \mu\text{g mL}^{-1}$ ); Ver-MSNs, verteporfin loaded mesoporous silica nanoparticles ( $10\ \mu\text{g mL}^{-1}$ ). Source: Figure taken with permission from (95).

to treat primary cutaneous melanoma lesions at early stages localized in the epidermis, the outermost layer of the skin (105,106).

To cite some examples of RB combined with silica nanoparticles, Chen *et al.* have encapsulated RB inside MSNs of 170 nm, together with the chemodrug Doxorubicin (DOX) for their delivery in murine mammary carcinoma (4T1) cells. The external surface of MSN was decorated with Hyaluronic acid (HA) as selective target for this type of cancer cell (RB-DOX@HMSNs-N=C-HA; [107]). Chen *et al.* demonstrated the importance of the use of nanoparticles coated with HA to enhance the drug delivery selectively into the cells of interest.

They tested the nanosystem and compared it with free RB and DOX in the 4T1 cells and 293 T cells, with and without overexpressed receptors, respectively (Fig. 12). RB and DOX were able to accumulate in both cell lines while RB-DOX@HMSNs-N=C-HA NPs were only internalized into 4T1 cell line. Moreover, when they incubated the nanoparticles together with HA free in the

culture media a low cellular uptake of MSN in the 4T1 was reached (Fig. 12d) denoting again the importance of the targeting strategies to enhance internalization (107).

They have tested the different cyto- and phototoxicity in 4T1 cells by incubating the following systems: (1) free RB, (2) RB@HMSNs-N=C-HA, (3) free DOX, (4) DOX@HMSNs-N=C-HA and (5) RB-DOX@HMSNs-N=C-HA. All the samples with DOX demonstrated a cytotoxic effect in dark conditions at even a low concentration ( $\text{IC}_{50} \approx 0.70\ \mu\text{g mL}^{-1}$ ). However, both free RB in solution and RB@HMSNs-N=C-HA were nontoxic in dark even at the highest nanoparticle concentration proving the lack of toxicity of RB and MSN without light. Concerning phototoxicity effects, RB and RB@HMSNs-N=C-HA showed similar  $\text{IC}_{50}$ , (9 and  $8.89\ \mu\text{g mL}^{-1}$ ) while the complete system in which chemo and phototherapy are combined displayed a higher effect with an  $\text{IC}_{50}$  of  $0.23\ \mu\text{g mL}^{-1}$ , indicating the advantage of the combination of two different approaches in the same MSN (107).

We have also worked on functionalized MSNs with RB in order to demonstrate an increase in the phototoxic action with respect to RB free in solution. The RB was anchored to the external surface of MSN with 50 nm of diameter together with polyethylene glycol (PEG) and Folic acid (FA) to enhance the stability in aqueous media and selectivity for cancer cells (79). For the anchorage of RB, two different synthesis routes were followed; RB was anchored at the amine groups of MSN and at the hydroxyl groups. As the number of  $-\text{OH}$  was considerably higher than  $-\text{NH}_2$ , the amount of RB linked was double for the second approach ( $20\ \mu\text{mol g}^{-1}$  vs  $10\ \mu\text{mol g}^{-1}$ ), being a more interesting system in terms of a lower amount ( $\text{mg kg}^{-1}$ ) of nanoparticles required. The systems displayed a high singlet oxygen production together with a modest but suitable fluorescence for bioimaging ( $\Phi_{\Delta} \approx 0.85$  and  $\Phi_{\text{f}} \approx 0.10$ , respectively) making them of potential interest to be used as theragnostic agents (imaging and therapy, Fig. 13). It has been previously demonstrated that these 50 nm diameter nanoparticles functionalized with PEG and FA but Rhodamine (RH101) as fluorophore instead of RB, are internalized into lysosomes of HeLa cells (36). Although RB has a lower fluorescence quantum yield in comparison with RH101, RB@MSNs can have enough brightness to be visualized by conventional fluorescence images whereas RB free in solution is faintly seen (Fig. 9). Besides,

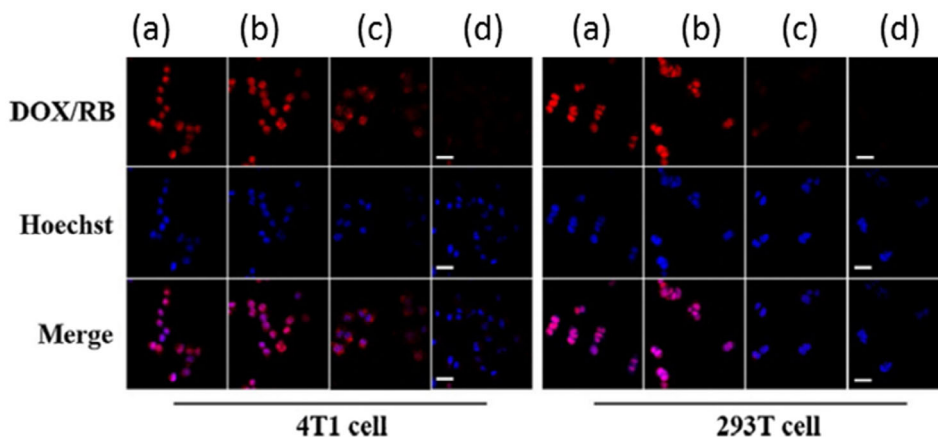


**Figure 12.** Confocal laser scanning microscope images of 4T1 (left) and 293T (right) cells coincubated with (a) free DOX, (b) DOX + RB, (c) RB-DOX@HMSNs-N=C-HA and (d) RB-DOX@HMSNs-N=C-HA + free HA for 4 h. Red fluorescence from DOX and RB, blue fluorescence from nuclei stained with Hoechst 33342, and the last overlays of blue fluorescence and red fluorescence. Scale bar:  $30\ \mu\text{m}$ . Source: Figure taken with permission from (107).

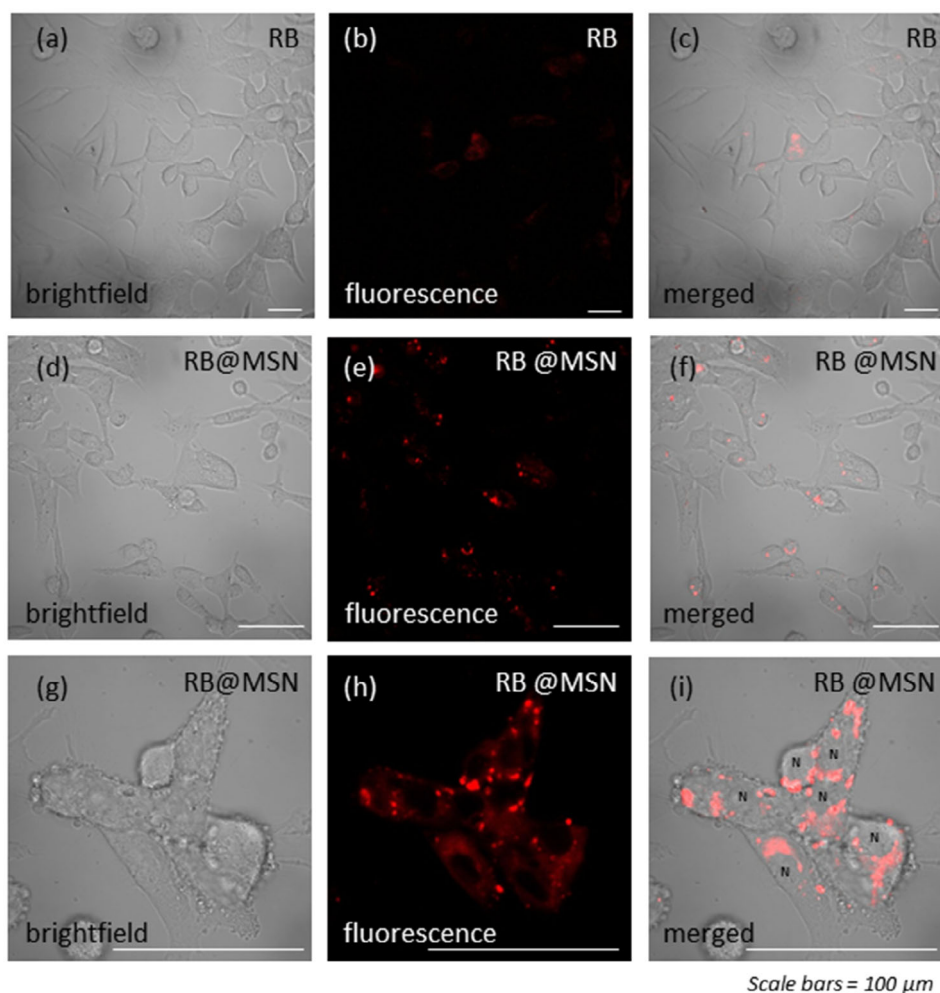


**Figure 13.** Bright field (left), fluorescence (middle) and merge (right) images of HeLa cells exposed to RB free in solution (a-c) and cells exposed to RB@MSN (d-i) at the same RB concentration (1  $\mu\text{M}$ ). Scale bars = 100  $\mu\text{m}$ . Source: Figure taken with permission from (79).

they demonstrated by RB@MSN in culture media that the phototoxicity action under green light at  $10 \text{ J cm}^{-2}$  was higher in comparison with the free RB, as shown in their  $\text{EC}_{50}$  in Table 2 (79).

### BODIPYs

Besides porphyrins and xanthenes-types, BODIPY dyes have emerged as a new family of PSs. Although this chromophore is more known as an excellent fluorophore, modifications of its structure have allowed the tunability of the photophysical properties, leading to suitable photosensitizers for PDT (11,12,108–113). Nevertheless, their poor solubility in water and the low selectivity for cancer cells can be improved by attaching hydrophilic and targeting groups at its molecular structure (109,114–117) or by the use of nanoparticles (24,98,115,118–122).

In this context, Zhu *et al.* (24) tethered an iodinated-BODIPY to the surface of the MSN of 90 nm diameter, coated also with PEG. They demonstrated the internalization of this nanosystem (MSN-I<sub>2</sub>-BDP-PEG) *in vitro* in HeLa cells at two different times of incubation (Fig. 14). According to these fluorescence microscopy images, the fluorescence increased with time indicating that the internalization of MSN-I<sub>2</sub>-BDP-PEG was time-dependent.

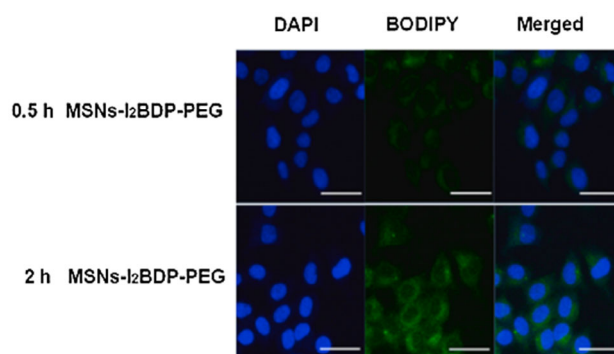


**Figure 14.** CLSM image of HeLa cells incubated with MSNs-I<sub>2</sub>BDP-PEG. On the left side, DAPI-stained nuclei showed blue fluorescence, BODIPY showed green fluorescence in cells, and the overlays of both images were shown on the rightmost. From top to bottom, it represented HeLa cells incubated with MSNs-I<sub>2</sub>BDP-PEG (0.5 and 2 h). Scale bar, 50  $\mu\text{m}$ . Source: Figure taken with permission from (24).

They studied the phototoxicity effect under green irradiation (500 nm;  $4.8 \text{ J cm}^{-2}$ ) in culture media. The nanosystem displayed a high effect under irradiation with an  $\text{IC}_{50} = 5 \mu\text{g mL}^{-1}$ . They demonstrated, by staining the live HeLa cells with calcein-

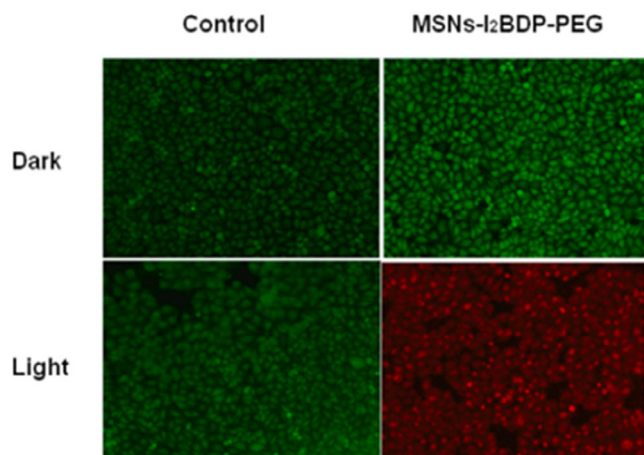


**Figure 15.** Fluorescence imaging of HeLa cells (Control, Control + Light, MSNs-I<sub>2</sub>BDP-PEG in dark and MSNs-I<sub>2</sub>BDP-PEG + Light). Cells were treated with live/dead staining: live cells were stained with calcein-AM to emit green fluorescence, and dead/late apoptotic cells were stained with propidium iodide (PI) to emit red fluorescence. Source: Figure taken with permission from (24).

AM (green fluorescence) and the dead/late apoptotic cells with propidium iodide, (PI, red fluorescence), that only the cells with MSN-I<sub>2</sub>-BDP-PEG previously irradiated showed red emission (Fig. 15), whereas MSN-I<sub>2</sub>-BDP-PEG in dark conditions did not show any toxicity (24).

Our group also studied a great number of BODIPYs anchored at the external surface of 50 nm diameter MSNs together with PEG-2000 and FA (79). BODIPYs with different absorption bands, from the blue to the red region, with iodine atoms in the structure and even halogen-free BODIPY (based on orthogonal dimers), have been tested (BDP-1, -2, -3, -4, -5, -6 and -7).

All PS-PEG-FA-MSNs were widely characterized. They revealed high singlet oxygen generation (higher than 50%) to the detriment of their fluorescence ability (lower than 5%) except for red-iodinated-BODIPY, which presented a noticeable fluorescence ( $\approx 20\%$ ). All the systems were tested *in vitro* in HeLa cells, by irradiating at their respective wavelengths depending on their absorption band (Fig. 16). The blue-BODIPY anchorage to the MSN (BDP1-NP) under 435 nm irradiation at  $10 \text{ J cm}^{-2}$ , was able to induce around 70% cell death at  $1 \mu\text{M}$  and near 90% cell death at  $5 \mu\text{M}$  ( $\text{EC}_{50} = 1.0 \mu\text{M}$ ), Table 2. Green-BODIPY nanosystem (BDP3-NP under a light exposure of 518 nm at  $10 \text{ J cm}^{-2}$ ) presented better performance reaching  $\geq 80\%$  phototoxicity at  $0.5 \mu\text{M}$  and  $\geq 90\%$  at  $1 \mu\text{M}$ , leading to  $\text{EC}_{50}$  of  $0.4 \mu\text{M}$  (Fig. 16, Table 2). Moreover, this BDP3-NP did not present cytotoxicity in dark conditions while its analog BODIPY-free in solution showed an  $\text{IC}_{50\text{dark}} \approx 4 \mu\text{M}$ . Therefore, the use of MSN contributes to the elimination of dark cytotoxicity of the iodinated-BODIPYs derivatives at higher concentrations. Concerning the green absorbing BODIPY dimer without halogen atoms did not show toxicity in dark, but its phototoxicity action was reduced when was incubated free in culture media in HeLa cells, assigned to the lack of solubility and poor internalization. However, its phototoxic effect was drastically enhanced when

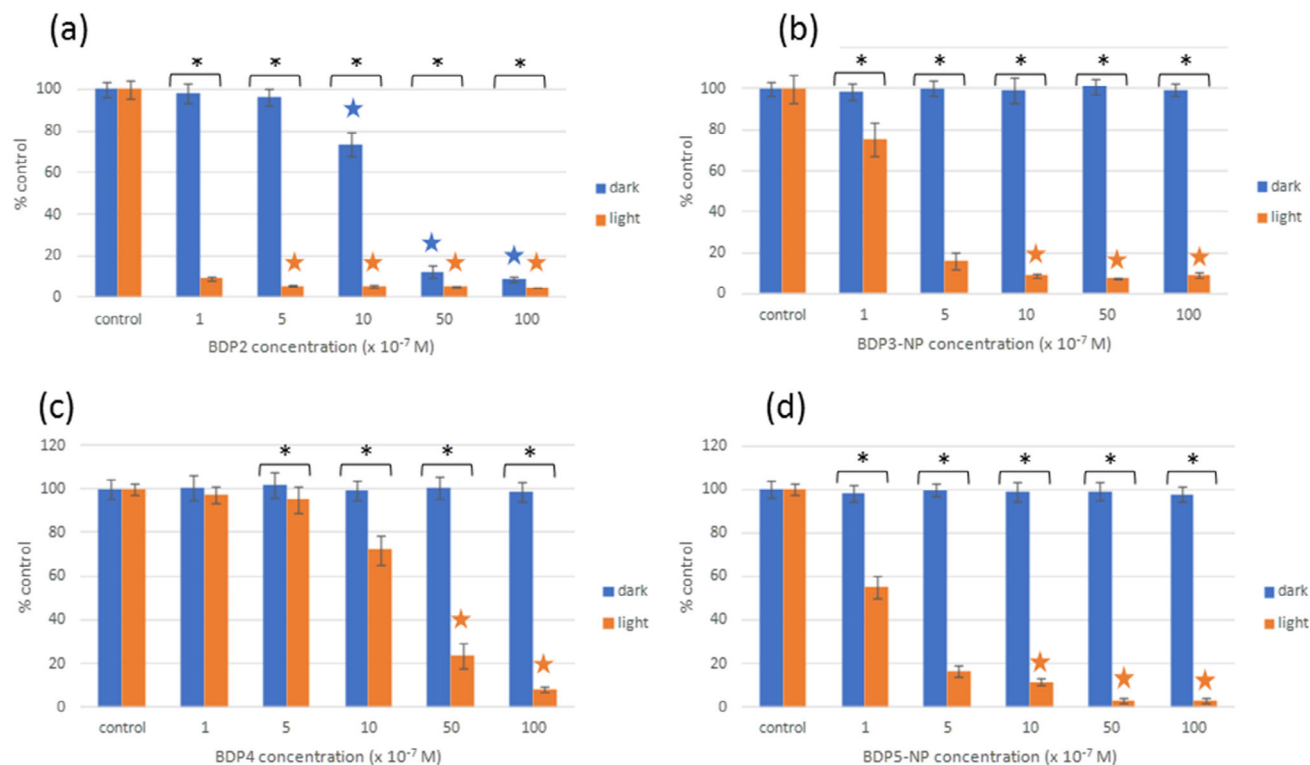


**Figure 16.** MTT assays of HeLa cells exposed to the PSs in solution: (a) BDP2 and (c) BDP4, and their corresponding nanosystems: (b) BDP3-NP and (d) BDP5-NP under dark conditions (blue bars) and after green irradiation at  $10 \text{ J cm}^{-2}$  (orange bars). Stars indicate significant differences with respect to controls. Asterisks indicate significant differences between dark and light conditions at the same concentrations tested. Source: Figure taken with permission from (79).

the BODIPY dimer was tethered at the MSN surface (BDP5-NP) reaching an  $EC_{50}$  value 40 times higher than that for the dimer-BODIPY in solution (Fig. 16 and Table 2; [79]).

Red-BODIPYs, the most interesting for potential PDT applicability, were also designed and attached to functionalized MSNs. BODIPY with red spectroscopic bands usually display lower oxygen singlet production compared with those with absorption bands in the green or blue region (11), but in this case, the phototoxicity singlet action is balanced with a higher absorption coefficient, accounted for Phototoxic Power factor ( $PP = \epsilon \times \Phi_{\Delta}$ ), which resulted in a low  $EC_{50} < 0.1 \mu\text{M}$  (Table 2; [79]). Note here, that once again a cytotoxic effect was obtained under dark conditions for iodinated-red-BODIPY-free ( $EC_{50} \approx 4 \mu\text{M}$ ) but it was not the case for the MSN loaded with those red-BODIPY. This system also endowed enough emission to be tracked by fluorescence microscopy in HeLa cells as shown in Fig. 17 (79).

### Others Photosensitizers

Other families of PS also have been used in PDT loaded in MSN (47,123,124). For instance, Zhou *et al.* encapsulated indocyanine green (ICG) together with Doxorubicin hydrochloride (DOX) inside MSNs. They prepared MSNs of 120 nm diameter and were externally decorated with Hyaluronic Acid (HA), a target for CD44 receptor (overexpressed on the surface of many tumor cells), increasing the final diameter size to 170 nm (47). They demonstrated the selectivity of their nanosystems by comparing the internalization into cancer cells (4T1) with respect to nontumoral cells (293T) in culture media. They recorded, on the one hand, how the free ICG and DOX were accumulated in both types of cells, and on the other hand, how the nanocarriers with HA coating were greater accumulated in the 4T1 cells than in the 293T cells. This group analyzed the biocompatibility of MSNs without the drugs, in dark and under light irradiation in cell culture.

Negligible cytotoxicity was displayed, obtaining around a 90% of the cell viability at the concentration of  $200 \mu\text{g mL}^{-1}$  (47). When they irradiated 4T1 cells previously incubated with the ID@HMSNs-B-HA for 5 min with 808 nm light ( $2 \text{ W cm}^{-2}$ ), an  $IC_{50}$  of  $1.35 \mu\text{g mL}^{-1}$  was obtained for this system but when the system did not contain DOX, this  $IC_{50}$  value drastically increased ( $>16 \mu\text{g mL}^{-1}$ ) likewise when the nanocarrier only contained DOX ( $IC_{50} = 32 \mu\text{g mL}^{-1}$ ), indicating the synergy in the combination of both drugs into the same MSNs (47).

Another type of PS is curcumin (Cur), which is extracted from *Curcuma longa*. It has diverse biological applications such

as an antioxidant, antidiabetic and also anticancer agent. Although it is not applicable PS for PDT in terms of its absorption range (band center at 425 nm), we have selected the work performed by Kuang *et al.* (123) as a proof of concept of how functionalized MSNs assisted the solubility in aqueous media and cell internalization of PS.

In this context, Cur was occluded into MSNs of 100 nm diameter and externally decorated with polyethylene glycol (PEG) MSN-PEG@Cur nanoparticles showed good stability in water and only a few NPs precipitated after 4 h of incubation, while the Cur free in solution is not water-soluble. *In vitro* assays indicated a good internalization of the MSN-PEG@Cur nanosystem, proven by the higher fluorescence intensity recorded with respect to that of free-Cur confocal laser scanning microscopy (Fig. 18; [123]).

The cytotoxicity and phototoxicity (under 430 nm irradiation at  $20 \text{ mW cm}^{-2}$  for 30 min), were evaluated by MTT assay for free-Cur and MSN-PEG@Cur after incubation at different concentrations (Fig. 19). Both systems were biosafety under dark conditions without any cytotoxic effect, but under irradiation, there were significant differences. Once again, MSN-PEG@Cur was considerably more efficient in terms of destroying HeLa cells than Cur Free, obtaining an  $IC_{50}$  4 times higher than when it was at MSNs (Fig. 19; [123]).

The last example of PSs is related to organometallic compounds, especially those based on Ru (II) polypyridine complexes (124, 125). Karges *et al.* were able to covalently link two derivatives of Ru (II) polypyridine complexes at the mesoporous silica nanoparticles of 200 nm diameter (124). In their work, although these compounds do not show proper bands for PDT (Table 2), the study is focused on the comparison of their toxicity under dark and light conditions free in solution and in combination with MSNs in presence and absence of Folic Acid as specific target for cancer cells. For that, they tested in culture media the cyto- and phototoxicity under irradiation of 480 nm at  $8.7 \text{ J cm}^{-2}$  or 540 nm at  $9.5 \text{ J cm}^{-2}$  of the four nanosystems in noncancerous human normal lung fibroblast (MRC5) cells and cancerous human ovarian carcinoma (A2780) cells, type of cells without and with overexpressed folate receptors, respectively. The results were compared with the Ru(II) complexes-free in solution.

The cytotoxic effect of the Ru(II) in dark conditions led to  $IC_{50,\text{dark}} = 23.7\text{--}38.1 \mu\text{M}$  in both cells line. This inherent toxicity was reduced when the Ru(II) was linked to MSN ( $IC_{50,\text{dark}} > 500 \mu\text{g mL}^{-1}$ ;  $>133\text{--}549 \text{ nm}$ ; [124]). Both Ru(II) complexes-free and anchorage in MSN but without Folic Acid displayed nonselectivity phototoxicity for cancerous cells

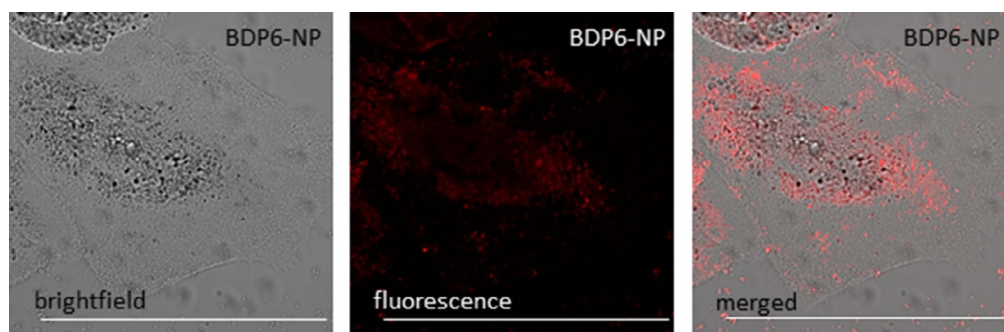


**Figure 17.** Brightfield (left), fluorescence (middle) and merge (right) images of HeLa cells treated with  $1 \mu\text{M}$  BDP6-NP for 24 h. Scale bars = 100  $\mu\text{m}$ . Source: Figure taken with permission from (79).

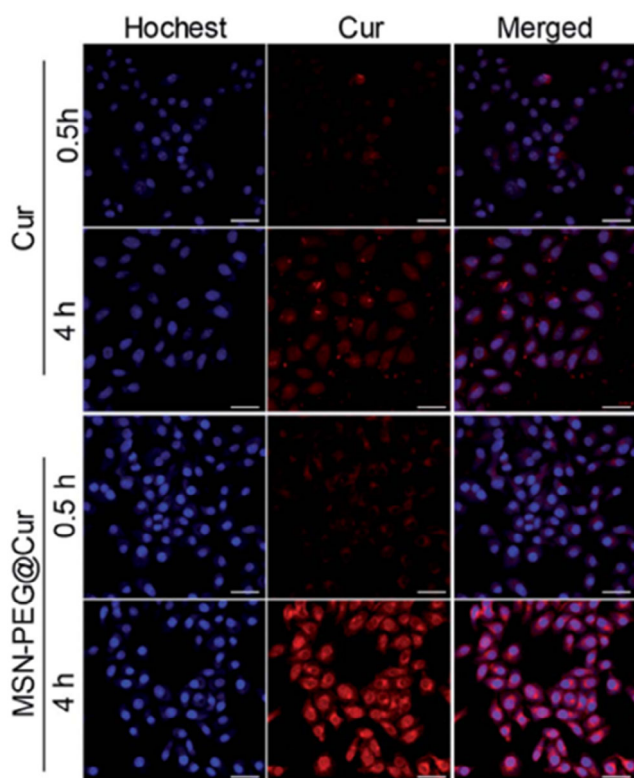


**Figure 18.** CLSM images of HeLa cells incubated with Cur or MSN-PEG@Cur for 0.5 and 4 h (scale bar = 50  $\mu\text{m}$ ). Source: Figure taken with permission from (123).

(Table 2). However, MSNs decorated with the FA have shown a marked difference in the internalization when noncancerous cell line (MRC-5) and cancerous cell line (A2780) were compared (Table 2) and as a consequence, selective phototoxicity for cancer cells was found (124).

Note here that all the *in vitro* studies presented in this review are performed by MMT assay, a colorimetric test used to measure mitochondrial function by the activity of NAD(P)H-dependent oxidoreductase enzymes as an indicator of cell viability. It has advantages such as versatility, simplicity, low cost and short duration. It is a powerful tool but it has limitations (126). For instance, as a single-point assay there is no information about the cells growth activity, and in some cases can underestimate the viability of cells (127–129). For this reason, it would

be recommended to apply different *in vitro* assays, as clonogenic assay (HTCA), commonly used to study survival of irradiated cancer cells, and it has a greater correlation with clinical response, to avoid misleading results and achieve a better reliability in the determination of cell survival to advance in PDT cancer treatment (130,131).

## CONCLUSIONS AND FUTURE PERSPECTIVES

This review underlines recent works related to mesoporous silica nanoparticles as photosensitizer carriers. As is described along this review, many PS-MSN are synthesized, characterized and tested *in vitro* and in some cases *in vivo*, but the multiple differences among them impede a proper comparison. The variety of the nanosystems includes: (1) the diameter size of the nanoparticles (from 50 to 200 nm), (2) the type of PSs, PS loading extension and methodology followed (encapsulated inside and/or tethered outside MANs), and final PS-MSN dosage incubation, (3) the different biotargets used to specifically bind to different overexpressed receptors (*i.e.* small molecules as folic acid or mannose, antibodies as human serum albumin, glycosaminoglycans as hyaluronic acid or xylan) as well as diverse cell lines (*i.e.* of skin, prostate, colorectal, breast, lung, cervical or ovarian cancer) and finally (5) the type of light sources and the irradiation doses, were generally different in each study.

However, we would like to highlight that all the cases in which PS was combined with MSNs have shown beneficial properties over the PS-free in solution. To mention the most important results, PS-MSN hybrid nanosystems were able to: (1) eliminate or minimize the cytotoxicity in dark conditions (2) increase their solubility and stability in physiological media, (3) enhance their selectivity and internalization in cancer cells, promoting antitumor PDT efficacy at lower PS amount incubated and ensuring safe use in clinical trials with respect the PS in solution.

Accordingly, MSNs with high surface areas, large pore sizes, simple and cost-effective synthesis and easy surface functionalization are considered potential nanoplatforms for targeting the delivery of PSs. Besides, they are able to combine different therapeutic treatments (photodynamic-, chemo- or photothermal-therapies), and provide imaging or diagnostic capabilities as well.

At this moment, to develop more efficient PS-MSN platforms, comprehensive and extensive studies to analyze their structure–

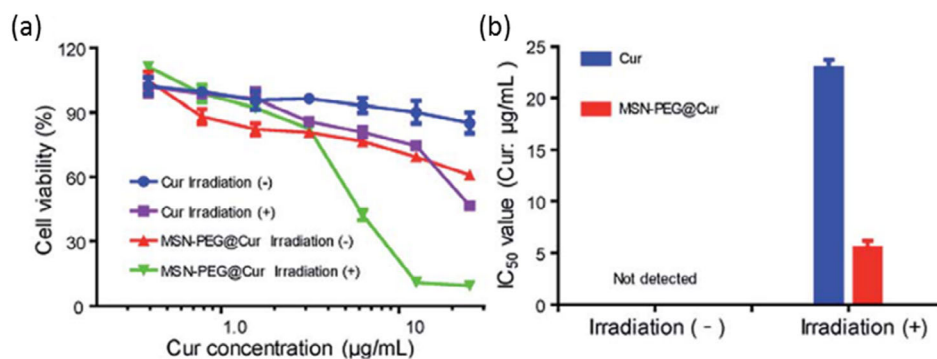


**Figure 19.** (a) *In vitro* assays of Cur in solution and MSN-PEG@Cur with or without irradiation against HeLa cells for 72 h; (b) IC<sub>50</sub> values of Cur (Cur  $\text{mg mL}^{-1}$ ) and MSN-PEG@Cur (Cur  $\text{mg mL}^{-1}$ ) against HeLa cells after 72 h of incubation with or without irradiation. Irradiation (–) indicates without irradiation. Irradiation (+) indicates irradiation. Source: Figure taken with permission from (123).

activity relationship, cyto- and phototoxicity, biocompatibility, biodistribution and excretion and dosages, by different *in vitro* assays (*i.e.* clonogenic assays as complementary to MTT assays) and *in vivo* (on different animal and human models), are required.

However, the lack of standardized protocols for their synthesis, (external and internal) surface modification, bioconjugation, and light sources and dosage leads to a poor reproducibility and makes difficult the assessment of their final biological action (under light and dark conditions), limiting their implementation in clinical trials. A systematic preparation, treatment and functionalization to control their morphology, particle and pore size, (photo)drug loading and its precise release at a target site, by selected strategies and model nanosystems will enhance their PDT applications. This complex challenge should be addressed by interdisciplinary scientific community to make the industrial translation a reality and reach the market in a near future.

The continuous advances in PS-MSNs validate their importance for future biomedical applications, providing a class of multifunctional nanoplatforams for PDT and other therapeutic and diagnostic applications. For all these reasons, we envisage a promising future of PS-MSNs coated with different targeting moieties in the application of PDT against cancer in clinical trials.

**Acknowledgements**—We gratefully acknowledge financial support from MCIN/AEI/10.13039/501100011033 (project PID2020-114347RB-C32), and Gobierno Vasco-Eusko Jaurlaritza (project IT1639-22). R.P.-M. thanks UPV/EHU, MIU and NGEU for their postdoctoral contract (MARSA21/71).

## REFERENCES

- Bray, F., J. Ferlay, I. Soerjomataram, R. L. Siegel, L. A. Torre and A. Jemal (2018) Global cancer statistics 2018: GLOBOCAN estimates of incidence and mortality worldwide for 36 cancers in 185 countries. *CA Cancer J. Clin.* **68**, 394–424.
- Siegel, R. L., K. D. Miller and A. Jemal (2020) Cancer statistics, 2020. *CA Cancer J. Clin.* **70**, 7–30.
- Lucky, S. S., K. C. Soo and Y. Zhang (2015) Nanoparticles in photodynamic therapy. *Chem. Rev.* **115**, 1990–2042.
- Chaturvedi, V. K., A. Singh, V. K. Singh and M. P. Singh (2018) Cancer nanotechnology: A new revolution for cancer diagnosis and therapy. *Curr. Drug Metab.* **20**, 416–429.
- Mirabello, V., D. G. Calatayud, R. L. Arrowsmith, H. Ge and S. I. Pascu (2015) Metallic nanoparticles as synthetic building blocks for cancer diagnostics: From materials design to molecular imaging applications. *J. Mater. Chem. B* **3**, 5657–5672.
- Bretin, L., A. Pinon, S. Bouramtane, C. Ouk, L. Richard, M. Perrin, A. Chaunavel and C. Carrion (2019) Photodynamic therapy activity of new human colorectal cancer. *Cancer* **11**, 1–27.
- Sarbadhikary, P., B. P. George and H. Abrahamse (2021) Recent advances in photosensitizers as multifunctional theranostic agents for imaging-guided photodynamic therapy of cancer. *Theranostics* **11**, 9054–9088.
- Qin, S., Y. Xu, H. Li, H. Chen and Z. Yuan (2022) Recent advances in *in situ* oxygen-generating and oxygen-replenishing strategies for hypoxic-enhanced photodynamic therapy. *Biomater. Sci.* **10**, 51–84.
- Smith, C. B., L. C. Days, D. R. Alajroush, K. Faye, Y. Khodour, S. J. Beebe and A. A. Holder (2022) Photodynamic therapy of inorganic complexes for the treatment of cancer†. *Photochem. Photobiol.* **98**, 17–41.
- Karges, J. (2022) Clinical development of metal complexes as photosensitizers for photodynamic therapy of cancer. *Angew. Chem. Int. Ed.* **61**, 1–9.
- Prieto-Montero, R., A. Prieto-Castañeda, A. Katsumiti, R. Sola-Llano, A. R. Agarrabeitia, M. P. Cajaraville, M. J. Ortiz and V. Martínez-Martínez (2022) Red haloBODIPYs as theragnostic agents: The role of the substitution at meso position. *Dyes Pigm.* **198**, 110015.
- Prieto-Montero, R., A. Prieto-Castañeda, R. Sola-Llano, A. R. Agarrabeitia, D. García-Fresnadillo, I. López-Arbeloa, A. Villanueva, M. J. Ortiz, S. Moya and V. Martínez-Martínez (2020) Exploring BODIPY derivatives as singlet oxygen photosensitizers for PDT. *Photochem. Photobiol.* **96**, 458–477.
- Dąbrowski, J. M. and L. G. Arnaut (2015) Photodynamic therapy (PDT) of cancer: From local to systemic treatment. *Photochem. Photobiol. Sci.* **14**, 1765–1780.
- Hopper, C. (2000) Photodynamic therapy: A clinical reality in the treatment of cancer. *Lancet Oncol.* **1**, 212–219.
- Moghissi, K., K. Dixon and S. Gibbins (2015) A surgical view of photodynamic therapy in oncology: A review. *Surg. J.* **1**, e1–e15.
- Lin, J. and M. T. Wan (2014) Current evidence and applications of photodynamic therapy in dermatology. *Clin. Cosmet. Investig. Dermatol.* **7**, 145–163.
- DeRosa, M. (2002) Photosensitized singlet oxygen and its applications. *Coord. Chem. Rev.* **233–234**, 351–371.
- Prieto-Montero, R., R. Sola-Llano, R. Montero, A. Longarte, T. Arbeloa, I. López-Arbeloa, V. Martínez-Martínez and S. Lacombe (2019) Methylthio BODIPY as a standard triplet photosensitizer for singlet oxygen production: A photophysical study. *Phys. Chem. Chem. Phys.* **21**, 20403–20414.
- Nonell, S. and C. Flors (2016). In *Singlet Oxygen, Applications in Biosciences and Nanosciences* (Edited by S. Nonell and C. Flors). Royal Society of Chemistry, Cambridge.
- Lacombe, S. and T. Pigot (2016) Materials for selective photo-oxygenation vs. photocatalysis: Preparation, properties and applications in environmental and health fields. *Catal. Sci. Technol.* **6**, 1571–1592.
- Stallivieri, A., L. Colombeau, G. Jetpisbayeva, A. Moussaron, B. Myrzakhmetov, P. Arnoux, S. Acherar, R. Vanderesse and C. Frochet (2017) Folic acid conjugates with photosensitizers for cancer targeting in photodynamic therapy: Synthesis and photophysical properties. *Bioorg. Med. Chem.* **25**, 1–10.
- Stephen, S., B. Gorain, H. Choudhury and B. Chatterjee (2022) Exploring the role of mesoporous silica nanoparticle in the development of novel drug delivery systems. *Drug Deliv. Transl. Res.* **12**, 105–123.
- Lee, D., S. Kwon, S. Jang, E. Young Park, Y. Lee and H. Koo (2022) Overcoming the obstacles of current photodynamic therapy in tumors using nanoparticles. *Bioact. Mater.* **8**, 20–34.
- Zhu, Y., N. Song, L. Chen and Z. Xie (2021) Reduction responsive BODIPY decorated mesoporous silica nanoscale platforms for photodynamic therapy. *Microporous Mesoporous Mater.* **311**, 110689–110678.
- Chauhan, P. and N. Yan (2016) Novel bodipy - cellulose nanohybrids for the production of singlet oxygen. *RSC Adv.* **6**, 32070–32073.
- Wu, H., W. Wang, Z. Zhang, J. Li, J. Zhao, Y. Liu, C. Wu, M. Huang, Y. Li and S. Wang (2020) Synthesis of a clay-based Nanoagent for Photonanomedicine. *ACS Appl. Mater. Interfaces* **12**, 390–399.
- Sargol Mazraedoost and Gity Behbudi (2021) Nano materials-based devices by photodynamic therapy for treating cancer applications. *J. Adv. Appl. NanoBio Tech.* **2**, 9–21.
- Dai, X., T. Du and K. Han (2019) Engineering nanoparticles for optimized photodynamic therapy. *ACS Biomater. Sci. Eng.* **5**, 6342–6354.
- Mousa, M., N. D. Evans, R. O. C. Oreffo and J. I. Dawson (2018) Clay nanoparticles for regenerative medicine and biomaterial design: A review of clay bioactivity. *Biomaterials* **159**, 204–214.
- Rudramurthy, G. R. and M. K. Swamy (2018) Potential applications of engineered nanoparticles in medicine and biology: An update. *JBIC J. Biol. Inorg. Chem.* **23**, 1185–1204.
- Jeevanandam, J., A. Barhoum, Y. S. Chan, A. Dufresne and M. K. Danquah (2018) Review on nanoparticles and nanostructured materials: History, sources, toxicity and regulations. *Beilstein J. Nanotechnol.* **9**, 1050–1074.
- Malvindi, M. A., V. Brunetti, G. Vecchio, A. Galeone, R. Cingolani and P. P. Pompa (2012) SiO<sub>2</sub> nanoparticles biocompatibility and their potential for gene delivery and silencing. *Nanoscale* **4**, 486–495.



33. Vallet-Regí, M. (2022) Our contributions to applications of mesoporous silica nanoparticles. *Acta Biomater.* **137**, 44–52.
34. Kiaee, G., N. Dimitrakakis, S. Sharifzadeh, H. Kim, R. K. Avery, K. M. Moghaddam, R. Haghniazi, E. P. Yalcintas, N. R. de Barros, S. Karamikamkar, A. Libanori, A. Khademhosseini and P. Khoshakhlagh (2022) Laponite-based nanomaterials for drug delivery. *Adv. Healthc. Mater.* **11**, 2102054.
35. Peerzade, S. A. M. A., N. Makarova and I. Sokolov (2021) Ultrabright fluorescent silica nanoparticles for dual pH and temperature measurements. *Nanomaterials (Basel)* **11**, 1–17.
36. Prieto-Montero, R., A. Katsumiti, M. P. Cajaraville, I. López-Arbeloa and V. Martínez-Martínez (2020) Functionalized fluorescent silica nanoparticles for bioimaging of cancer cells. *Sensors* **20**, 5590.
37. Alexis, F., E. Pridgen, L. K. Molnar and O. C. Farokhzad (2008) Factors affecting the clearance and biodistribution of polymeric nanoparticles. *Mol. Pharm.* **5**, 505–515.
38. Mai, W. X. and H. Meng (2013) Mesoporous silica nanoparticles: A multifunctional nano therapeutic system. *Integr. Biol.* **5**, 19–28.
39. Pérez-Herrero, E. and A. Fernández-Medarde (2015) Advanced targeted therapies in cancer: Drug nanocarriers, the future of chemotherapy. *Eur. J. Pharm. Biopharm.* **93**, 52–79.
40. Bobo, D., K. J. Robinson, J. Islam, K. J. Thurecht and S. R. Corrie (2016) Nanoparticle-based medicines: A review of FDA-approved materials and clinical trials to date. *Pharm. Res.* **33**, 2373–2387.
41. Bharathiraja, S., M. S. Moorthy, P. Manivasagan, H. Seo, K. D. Lee and J. Oh (2017) Chlorin e6 conjugated silica nanoparticles for targeted and effective photodynamic therapy. *Photodiagnosis Photodyn. Ther.* **19**, 212–220.
42. Ribeiro, T., T. J. V. Prazeres, M. Moffitt and J. P. S. Farinha (2013) Enhanced photoluminescence from micellar assemblies of cadmium sulfide quantum dots and gold nanoparticles. *J. Phys. Chem. C* **117**, 3122–3133.
43. Pérez, N., L. Ruiz-Rubio, J. L. Vilas, M. Rodríguez, V. Martínez-Martínez and L. M. León (2016) Synthesis and characterization of near-infrared fluorescent and magnetic iron zero-valent nanoparticles. *J. Photochem. Photobiol. A Chem.* **315**, 1–7.
44. Zhuang, Y., L. Zhao, L. Zheng, Y. Hu, L. Ding, X. Li, C. Liu, J. Zhao, X. Shi and R. Guo (2017) LAPONITE-polyethylenimine based theranostic nanopatform for tumor-targeting CT imaging and chemotherapy. *ACS Biomater. Sci. Eng.* **3**, 431–442.
45. Martínez-Carmona, M., D. Lozano, A. Baeza, M. Colilla and M. Vallet-Regí (2017) A novel visible light responsive nanosystem for cancer treatment. *Nanoscale* **9**, 15967–15973.
46. Wu, S.-H., C.-Y. Mou and H.-P. Lin (2013) Synthesis of mesoporous silica nanoparticles. *Chem. Soc. Rev.* **42**, 3862.
47. Zhou, Y., C. Chang, Z. Liu, Q. Zhao, Q. Xu, C. Li, Y. Chen, Y. Zhang and B. Lu (2021) Hyaluronic acid-functionalized hollow mesoporous silica nanoparticles as pH-sensitive Nanocarriers for cancer chemo-photodynamic therapy. *Langmuir* **37**, 2619–2628.
48. Rastegari, E., Y. J. Hsiao, W. Y. Lai, Y. H. Lai, T. C. Yang, S. J. Chen, P. I. Huang, S. H. Chiou, C. Y. Mou and Y. Chien (2021) An update on mesoporous silica nanoparticle applications in nanomedicine. *Pharmaceutics* **13**, 1–56.
49. Martinelli, C., C. Pucci and G. Ciofani (2019) Nanostructured carriers as innovative tools for cancer diagnosis and therapy. *APL Bioeng.* **3**, 11502.
50. de Freitas, F. L. (2021) Nanomaterials for enhanced photodynamic therapy - From Basic Science to Clinical Research. *IntechOpen* **32**, 137–144.
51. Lü, J.-M., X. Wang, C. Marin-Muller, H. Wang, P. H. Lin, Q. Yao and C. Chen (2009) Current advances in research and clinical applications of PLGA-based nanotechnology. *Expert Rev. Mol. Diagn.* **9**, 325–341.
52. Sinha, R. P. and D. P. Häder (2002) UV-induced DNA damage and repair: A review. *Photochem. Photobiol. Sci.* **1**, 225–236.
53. Yu, S. L. and S. K. Lee (2017) Ultraviolet radiation: DNA damage, repair, and human disorders. *Mol. Cell. Toxicol.* **13**, 21–28.
54. Rastogi, R. P., K. A. Richa, M. B. Tyagi and R. P. Sinha (2010) Molecular mechanisms of ultraviolet radiation-induced DNA damage and repair. *J. Nucleic Acids* **2010**, 1–32.
55. Krajczewski, J., K. Rucińska, H. E. Townley and A. Kudelski (2019) Role of various nanoparticles in photodynamic therapy and detection methods of singlet oxygen. *Photodiagnosis Photodyn. Ther.* **26**, 162–178.
56. Stöber, W., A. Fink and E. Bohn (1968) Controlled growth of monodisperse silica spheres in the micron size range. *J. Colloid Interface Sci.* **26**, 62–69.
57. Zhang, Q. Y., W. X. Que, S. Buddhudu and K. Pita (2002) An efficient lasing action from pyromethene 556 dye-doped organically modified silicates. *J. Phys. Chem. Solid* **63**, 1723–1727.
58. Cheng, S.-H., C.-H. Lee, C.-S. Yang, F.-G. Tseng, C.-Y. Mou and L.-W. Lo (2009) Mesoporous silica nanoparticles functionalized with an oxygen-sensing probe for cell photodynamic therapy: Potential cancer theranostics. *J. Mater. Chem.* **19**, 1252–1257.
59. Lin, Y.-S. and C. L. Haynes (2010) Impacts of mesoporous silica nanoparticle size, pore ordering, and pore integrity on hemolytic activity. *J. Am. Chem. Soc.* **132**, 4834–4842.
60. Siddiqui, B., A. u. Rehman, I. Haq, A. A. Al-Dossary, A. Elaissari and N. Ahmed (2022) Exploiting recent trends for the synthesis and surface functionalization of mesoporous silica nanoparticles towards biomedical applications. *Int. J. Pharm.* **4**, 100116.
61. Galabova, B. B. (2022) Mesoporous silica nanoparticles: Synthesis, functionalization, drug loading and release - A review. *Trop. J. Pharm. Res.* **20**, 1091–1100.
62. Singh, P., S. Srivastava and S. K. Singh (2019) Nanosilica: Recent progress in synthesis, functionalization, biocompatibility, and biomedical applications. *ACS Biomater. Sci. Eng.* **5**, 4882–4898.
63. Ghaferi, M., K. M. M. Esfahani, A. Raza, S. Al Harthi, H. Ebrahimi Shahmabadi and S. E. Alavi (2021) Mesoporous silica nanoparticles: Synthesis methods and their therapeutic use-recent advances. *J. Drug Target.* **29**, 131–154.
64. Vallet-Regí, M., A. Rámila, R. P. del Real and J. Pérez-Pariente (2001) A new property of MCM-41: Drug delivery system. *Chem. Mater.* **13**, 308–311.
65. Chen, S., S. L. Greasley, Z. Y. Ong, P. Naruphontjirakul, S. J. Page, J. V. Hanna, A. N. Redpath, O. Tsigkou, S. Rankin, M. P. Ryan, A. E. Porter and J. R. Jones (2020) Biodegradable zinc-containing mesoporous silica nanoparticles for cancer therapy. *Mater. Today Adv.* **6**, 100066.
66. Burns, A., H. Ow and U. Wiesner (2006) Fluorescent core-shell silica nanoparticles: Towards 'lab on a particle' architectures for nano-biotechnology. *Chem. Soc. Rev.* **35**, 1028–1042.
67. Urata, C., Y. Aoyama, A. Tonegawa, Y. Yamauchi and K. Kuroda (2009) Dialysis process for the removal of surfactants to form colloidal mesoporous silica nanoparticles. *Chem. Commun.* **5094**, 5094–5096.
68. Zhang, Q., F. Liu, K. T. Nguyen, X. Ma, X. Wang, B. Xing and Y. Zhao (2012) Multifunctional mesoporous silica nanoparticles for cancer-targeted and controlled drug delivery. *Adv. Funct. Mater.* **22**, 5144–5156.
69. Martins Estevão, B., I. Miletto, L. Marchese and E. Gianotti (2016) Optimized Rhodamine B labeled mesoporous silica nanoparticles as fluorescent scaffolds for the immobilization of photosensitizers: A theranostic platform for optical imaging and photodynamic therapy. *Phys. Chem. Chem. Phys.* **18**, 9042–9052.
70. Manzano, M. and M. Vallet-Regí (2018) Mesoporous silica nanoparticles in nanomedicine applications. *J. Mater. Sci. Mater. Med.* **29**, 65.
71. Villaverde, G., A. Baeza, G. J. Melen, A. Alfranca, M. Ramirez and M. Vallet-Regí (2015) A new targeting agent for the selective drug delivery of nanocarriers for treating neuroblastoma. *J. Mater. Chem. B* **3**, 4831–4842.
72. Maurel, M., T. Montheil, J. Martin, L. Chaar, V. Guzman-Gonzalez, M. Couvet, T. Jacquet, T. Jia, B. Eymin, K. Parra, P. Dumy, J. Martinez, F. Ruggiero, E. Vaganay, A. Mehdi, J. L. Coll and G. Subra (2021) Design of pegylated three ligands silica nanoparticles for multi-receptor targeting. *Nanomaterials (Basel)* **11**, 1–23.
73. Son, J., S. M. Yang, G. Yi, Y. J. Roh, H. Park, J. M. Park, M. Choi and H. Koo (2018) Folate-modified PLGA nanoparticles for tumor-targeted delivery of pheophorbide a in vivo. *Biochem. Biophys. Res. Commun.* **498**, 523–528.
74. Freitas, L. B. D. O., I. J. G. Bravo, W. A. D. A. Macedo and E. M. B. De Sousa (2016) Mesoporous silica materials functionalized with folic acid: Preparation, characterization and release profile study with methotrexate. *J. Sol-Gel Sci. Technol.* **77**, 186–204.

75. Llinàs, M. C. and D. Sánchez-garcía (2014) Nanopartículas de sílice: preparación y aplicaciones en biomedicina. *Affinidad* **LXXI**, 20–31.
76. Ow, H., D. R. Larson, M. Srivastava, B. a. Baird, W. W. Webb and U. Wiesner (2005) Bright and stable core-shell fluorescent silica nanoparticles. *Nano Lett.* **5**, 113–117.
77. Wang, Z., X. Hong, S. Zong, C. Tang, Y. Cui and Q. Zheng (2015) BODIPY-doped silica nanoparticles with reduced dye leakage and enhanced singlet oxygen generation. *Sci. Rep.* **5**, 12602–12612.
78. Van Zundert, I., M. Bravo, O. Deschaume, P. Cybulski, C. Bartic, J. Hofkens, H. Uji-I, B. Fortuni and S. Rocha (2021) Versatile and robust method for antibody conjugation to nanoparticles with high targeting efficiency. *Pharmaceutics* **13**, 2153.
79. Prieto-Montero, R., A. Prieto-Castañeda, A. Katsumi, M. P. Cajaraville, A. R. Agarrabeitia, M. J. Ortiz and V. Martínez-Martínez (2021) Functionalization of photosensitized silica nanoparticles for advanced photodynamic therapy of cancer. *Int. J. Mol. Sci.* **22**, 6618–6641.
80. Tada, D. B. and M. S. Baptista (2015) Photosensitizing nanoparticles and the modulation of ROS generation. *Front. Chem.* **3**, 1–14.
81. Fu, C., T. Liu, L. Li, H. Liu, D. Chen and F. Tang (2013) The absorption, distribution, excretion and toxicity of mesoporous silica nanoparticles in mice following different exposure routes. *Biomaterials* **34**, 2565–2575.
82. He, X., H. Nie, K. Wang, W. Tan, X. Wu and P. Zhang (2008) In vivo study of biodistribution and urinary excretion of surface-modified silica nanoparticles. *Anal. Chem.* **80**, 9597–9603.
83. Lu, J., M. Liong, Z. Li, J. I. Zink and F. Tamanoi (2010) Biocompatibility, biodistribution, and drug-delivery efficiency of mesoporous silica nanoparticles for cancer therapy in animals. *Small* **6**, 1794–1805.
84. Fu, Q., D. Hargrove and X. Lu (2016) Improving paclitaxel pharmacokinetics by using tumor-specific mesoporous silica nanoparticles with intraperitoneal delivery. *Nanomedicine* **12**, 1951–1959.
85. Hussain, S. M., L. K. Braydich-Stolle, A. M. Schrand, R. C. Muddock, K. O. Yu, D. M. Mattie and J. J. Schlager (2009) Toxicity evaluation for safe use of nanomaterials: Recent achievements and technical challenges. *Adv. Mater.* **21**, 1549–1559.
86. Dougherty, T. J., G. B. Grindey, R. Fiel, K. R. Weishaupt and D. G. Boyle (1975) Photoradiation therapy. II. Cure of animal tumors with hematoporphyrin and light. *J. Natl. Cancer Inst.* **55**, 115–121.
87. Dougherty, T. J., G. Lawrence, J. Kenneth, R. Weishaupt and A. Goldfarb (1979) Photoradiation in the treatment of recurrent breast carcinoma. *J. Natl. Cancer Inst.* **62**, 231–237.
88. Dougherty, T. J., G. B. Grindey, R. Fiel, K. R. Weishaupt, D. G. Boyle, J. E. Kaufman, A. Goldfarb, K. R. Weishaupt, D. G. Boyle, A. Mittleman, G. Lawrence, J. Kenneth, R. Weishaupt and A. Goldfarb (1975) Photoradiation therapy for the treatment of malignant tumors. *J. Natl. Cancer Inst.* **38**, 231–237.
89. Bouffard, E., C. Mauriello Jimenez, K. El Cheikh, M. Maynadier, I. Basile, L. Raehm, C. Nguyen, M. Gary-Bobo, M. Garcia, J.-O. Durand and A. Morère (2019) Efficient photodynamic therapy of prostate cancer cells through an improved targeting of the cation-independent mannose 6-phosphate receptor. *Int. J. Mol. Sci.* **20**, 2809.
90. Bouramtane, S., L. Bretin, A. Pinon, D. Leger, B. Liagre, L. Richard, F. Brégier, V. Sol and V. Chaleix (2019) Porphyrin-xylan-coated silica nanoparticles for anticancer photodynamic therapy. *Carbohydr. Polym.* **213**, 168–175.
91. Li, S., Y. Zhang, X.-W. He, W.-Y. Li and Y.-K. Zhang (2020) Multifunctional mesoporous silica nanopatform based on silicon nanoparticles for targeted two-photon-excited fluorescence imaging-guided chemo/photodynamic synergetic therapy in vitro. *Talanta* **209**, 120552.
92. Vallet-Regí, M., M. Colilla, I. Izquierdo-Barba and M. Manzano (2018) Mesoporous silica nanoparticles for drug delivery: Current insights. *Molecules* **23**, 1–19.
93. Santiago, A. M., T. Ribeiro, A. S. Rodrigues, B. Ribeiro, R. F. M. Frade, C. Baleizão and J. P. S. Farinha (2015) Multifunctional hybrid silica nanoparticles with a fluorescent core and active targeting shell for fluorescence imaging biodiagnostic applications. *Eur. J. Inorg. Chem.* **2015**, 4579–4587.
94. Yang, L., J. Wang, S. Yang, Q. Lu, P. Li and N. Li (2019) Rod-shape MSN@MoS<sub>2</sub> nanopatform for FL/MSOT/CT imaging-guided photothermal and photodynamic therapy. *Theranostics* **9**, 3992–4005.
95. Rizzi, M., S. Tonello, B. M. Estevão, E. Gianotti, L. Marchese and F. Renò (2017) Verteporfin based silica nanoparticle for in vitro selective inhibition of human highly invasive melanoma cell proliferation. *J. Photochem. Photobiol. B Biol.* **167**, 1–6.
96. Joffre, C., R. Barrow, L. Ménard, V. Calleja, I. R. Hart and S. Kermorgant (2011) A direct role for met endocytosis in tumorigenesis. *Nat. Cell Biol.* **13**, 827–837.
97. Sánchez-Arroyo, A. J., E. Palao, A. R. Agarrabeitia, M. J. Ortiz and D. García-Fresnadillo (2017) Towards improved halogenated BODIPY photosensitizers: Clues on structural designs and heavy atom substitution patterns. *Phys. Chem. Chem. Phys.* **19**, 69–72.
98. González-Béjar, M., M. Liras, L. Francés-Soriano, V. Voliani, V. Herranz-Pérez, M. Duran-Moreno, J. M. Garcia-Verdugo, E. I. Alarcon, J. C. Scaiano and J. Pérez-Prieto (2014) NIR excitation of upconversion nanohybrids containing a surface grafted Bodipy induces oxygen-mediated cancer cell death. *J. Mater. Chem. B* **2**, 4554–4563.
99. Zhao, J., K. Xu, W. Yang, Z. Wang and F. Zhong (2015) The triplet excited state of Bodipy: Formation, modulation and application. *Chem. Soc. Rev.* **44**, 8904–8939.
100. Martínez, C. G., A. M. Braun and E. Oliveros (2004) Effect of the media on the quantum yield of singlet oxygen ( $O_2(^1\Delta_g)$ ) production by 9H-Fluoren-9-one: Microheterogeneous systems. *Helv. Chim. Acta* **87**, 382–393.
101. Bassan, E., A. Gualandi, P. G. Cozzi and P. Ceroni (2021) Design of BODIPY dyes as triplet photosensitizers: Electronic properties tailored for solar energy conversion, photoredox catalysis and photodynamic therapy. *Chem. Sci.* **12**, 6607–6628.
102. Banfi, S., E. Caruso, S. Zaza, M. Mancini, M. B. Gariboldi and E. Monti (2012) Synthesis and photodynamic activity of a panel of BODIPY dyes. *J. Photochem. Photobiol. B Biol.* **114**, 52–60.
103. Filatov, M. A., S. Karuthedath, P. M. Polestshuk, S. Callaghan, K. J. Flanagan, T. Wiesner, F. Laquai and M. O. Senge (2018) BODIPY-pyrene and perylene dyads as heavy-atom-free singlet oxygen sensitizers. *ChemPhotoChem* **2**, 606–615.
104. Demartis, S., G. Rassu, S. Murgia, L. Casula, P. Giunchedi and E. Gavini (2021) Improving dermal delivery of Rose Bengal by deformable lipid nanovesicles for topical treatment of melanoma. *Mol. Pharm.* **18**, 4046–4057.
105. Dhillon, S. K., S. L. Porter, N. Rizk, Y. Sheng, T. McKaig, K. Burnett, B. White, H. Nesbitt, R. N. Matin, A. P. McHale, B. Callan and J. F. Callan (2020) Rose Bengal-amphiphilic peptide conjugate for enhanced photodynamic therapy of malignant melanoma. *J. Med. Chem.* **63**, 1328–1336.
106. Maker, A. V., B. Prabhakar and K. Pardiwala (2015) The potential of Intralosomal rose Bengal to stimulate T-cell mediated anti-tumor responses. *J. Clin. Cell. Immunol.* **6**, 139–148.
107. Chen, K., C. Chang, Z. Liu, Y. Zhou, Q. Xu, C. Li, Z. Huang, H. Xu, P. Xu and B. Lu (2020) Hyaluronic acid targeted and pH-responsive nanocarriers based on hollow mesoporous silica nanoparticles for chemo-photodynamic combination therapy. *Colloids Surf. B Biointerfaces* **194**, 111166–111172.
108. Quan, Y., Q.-Y. Li, Q. Zhang, W.-Q. Zhang, H. Lu, J.-H. Yu, J. Chen, X. Zhao and X.-J. Wang (2016) A diiodo-BODIPY postmodified metal-organic framework for efficient heterogeneous organophotocatalysis. *RSC Adv.* **6**, 23995–23999.
109. Liu, J.-Y., P.-Z. Zhou, J.-L. Ma and X. Jia (2018) Trifluoromethyl boron dipyrromethene derivatives as potential photosensitizers for photodynamic therapy. *Molecules* **23**, 458–471.
110. Nguyen, V. N., Y. Yan, J. Zhao and J. Yoon (2021) Heavy-atom-free photosensitizers: From molecular design to applications in the photodynamic therapy of cancer. *Acc. Chem. Res.* **54**, 207–220.
111. Agazzi, M. L., M. B. Ballatore, A. M. Durantini, E. N. Durantini and A. C. Tomé (2019) BODIPYs in antitumoral and antimicrobial photodynamic therapy: An integrating review. *J. Photochem. Photobiol. C Photochem. Rev.* **40**, 21–48.
112. Awuah, S. G. and Y. You (2012) Boron dipyrromethene (BODIPY)-based photosensitizers for photodynamic therapy. *RSC Adv.* **2**, 11169–11183.

113. Kamkaew, A., S. H. Lim, H. B. Lee, L. V. Kiew, L. Y. Chung and K. Burgess (2013) BODIPY dyes in photodynamic therapy. *Chem. Soc. Rev.* **42**, 77–88.
114. Blázquez-Moraleja, A., L. Maierhofer, E. Mann, R. Prieto-Montero, A. Oliden-Sánchez, L. Celada, V. Martínez-Martínez, M. D. Chiara and J. L. Chiara (2022) Acetoxymethyl-BODIPY dyes: A universal platform for the fluorescent labeling of nucleophiles. *Org. Chem. Front.* **9**, 5774–5789.
115. Wang, J. L., L. Zhang, M. J. Zhao, T. Zhang, Y. Liu and F. L. Jiang (2021) Mitochondria-targeted BODIPY nanoparticles for enhanced Photothermal and photoacoustic imaging in vivo. *ACS Appl. Bio Mater.* **4**, 1760–1770.
116. Verwilt, P., C. C. David, V. Leen, J. Hofkens, P. A. M. De Witte and W. M. De Borggraeve (2013) Synthesis and in vitro evaluation of a PDT active BODIPY-NLS conjugate. *Bioorg. Med. Chem. Lett.* **23**, 3204–3207.
117. Ke, M. R., S. L. Yeung, D. K. P. Ng, W. P. Fong and P. C. Lo (2013) Preparation and in vitro photodynamic activities of folate-conjugated distyryl boron dipyrromethene based photosensitizers. *J. Med. Chem.* **56**, 8475–8483.
118. Guan, Q., L. Le Zhou, Y. A. Li and Y. B. Dong (2018) Diiodo-Bodipy-encapsulated nanoscale metal-organic framework for pH-driven selective and mitochondria targeted photodynamic therapy. *Inorg. Chem.* **57**, 10137–10145.
119. Li, M., X. Li, Z. Cao, Y. Wu, J. A. Chen, J. Gao, Z. Wang, W. Guo and X. Gu (2018) Mitochondria-targeting BODIPY-loaded micelles as novel class of photosensitizer for photodynamic therapy. *Eur. J. Med. Chem.* **157**, 599–609.
120. Sun, W., X. Zhao, J. Fan, J. Du and X. Peng (2019) Boron dipyrromethene nano-photosensitizers for anticancer phototherapies. *Small* **15**, 1804927–1804952.
121. Hu, W., H. Ma, B. Hou, H. Zhao, Y. Ji, R. Jiang, X. Hu, X. Lu, L. Zhang, Y. Tang, Q. Fan and W. Huang (2016) Engineering lysosome-targeting BODIPY nanoparticles for photoacoustic imaging and photodynamic therapy under near-infrared light. *ACS Appl. Mater. Interfaces* **8**, 12039–12047.
122. Lin, W., W. Zhang, S. Liu, Z. Li, X. Hu, Z. Xie, C. Duan and G. Han (2019) Engineering pH-responsive BODIPY nanoparticles for tumor selective multimodal imaging and phototherapy. *ACS Appl. Mater. Interf.* **11**, 43928–43935.
123. Kuang, G., Q. Zhang, S. He and Y. Liu (2020) Curcumin-loaded PEGylated mesoporous silica nanoparticles for effective photodynamic therapy. *RSC Adv.* **10**, 24624–24630.
124. Karges, J., D. Díaz-García, S. Prashar, S. Gómez-Ruiz and G. Gasser (2021) Ru(II) Polypyridine complex-functionalized mesoporous silica nanoparticles as photosensitizers for cancer targeted photodynamic therapy. *ACS Appl. Bio Mater.* **4**, 4394–4405.
125. Ellahoui, Y., M. Patra, C. Mari, R. Kaabi, J. Karges, G. Gasser and S. Gómez-Ruiz (2019) Mesoporous silica nanoparticles functionalised with a photoactive ruthenium(II) complex: Exploring the formulation of a metal-based photodynamic therapy photosensitizer. *Dalton Trans.* **48**, 5940–5951.
126. Ghasemi, M., T. Turnbull, S. Sebastian and I. Kempson (2021) The mtt assay: Utility, limitations, pitfalls, and interpretation in bulk and single-cell analysis. *Int. J. Mol. Sci.* **22**, 12827.
127. Kawada, K., T. Yonei, H. Ueoka, K. Kiura, M. Tabata, N. Takigawa, M. Harada and M. Tanimoto (2002) Comparison of chemosensitivity tests: Clonogenic assay versus MTT assay. *Acta Med. Okayama* **56**, 129–134.
128. Nikzad, S. and P. N. Milad Baradaran-Ghahfarokhi (2014) Dose-response modeling using MTT assay: A short review. *Life Sci. J.* **11**, 432–437.
129. Fotakis, G. and J. A. Timbrell (2006) In vitro cytotoxicity assays: Comparison of LDH, neutral red, MTT and protein assay in hepatoma cell lines following exposure to cadmium chloride. *Toxicol. Lett.* **160**, 171–177.
130. Buch, K., T. Peters, T. Nawroth, M. Sängler, H. Schmidberger and P. Langguth (2012) Determination of cell survival after irradiation via clonogenic assay versus multiple MTT assay - a comparative study. *Radiat. Oncol.* **7**, 1–6.
131. Xue, L. Y., S. M. Chiu and N. L. Oleinick (2001) Photodynamic therapy-induced death of MCF-7 human breast cancer cells: A role

for caspase-3 in the late steps of apoptosis but not for the critical lethal event. *Exp. Cell Res.* **263**, 145–155.

## AUTHOR BIOGRAPHIES



**Ruth Prieto-Montero** is a Postdoctoral Researcher at the Physical Chemistry Department of the Basque Country (UPV-EHU). She research is focused on the photophysical characterization of new fluorescence and photosensitizers dyes, together with the synthesis of inorganic and organic nanoparticles and their postfunctionalization to be used in biomedical applications (fluorescence imaging and photodynamic therapy).



**Teresa Arbeloa** is Associated Professor at the Physical Chemistry Department of the University of the Basque Country (UPV-EHU). Her interest is centered in computational simulations and photophysical characterization of molecular bioprobes; and multifunctional materials and dyes for biomedical and photonic applications.



**Virginia Martínez** is a Tenured Researcher at the Physical Chemistry Department at University of the Basque Country (UPV-EHU), Spain. She does research in Materials Chemistry and Spectroscopy. Her current projects are: (1) Photoactive hybrid materials for optical applications; (2) Multifunctional dyes as fluorescent biomarkers and new photosensitizers; and 3. Functionalized

nanoparticles for bioapplications, mainly Photodynamic Therapy.